

25

REPORT DOCUMENTATION PAGE

Form Approved  
OMB No. 0704-0188

The public reporting burden for this collection of information is estimated to average 1 hour per response, including the time for reviewing instructions, searching existing data sources, gathering and maintaining the data needed, and completing and reviewing the collection of information. Send comments regarding this burden estimate or any other aspect of this collection of information, including suggestions for reducing the burden, to the Department of Defense, Executive Services and Communications Directorate (0704-0188). Respondents should be aware that notwithstanding any other provision of law, no person shall be subject to any penalty for failing to comply with a collection of information if it does not display a currently valid OMB control number.

PLEASE DO NOT RETURN YOUR FORM TO THE ABOVE ORGANIZATION.

1. REPORT DATE (DD-MM-YYYY) 12-07-2006  
2. REPORT TYPE Final Report  
3. DATES COVERED (From - To) July 15, 2000 - December 31, 2005

4. TITLE AND SUBTITLE  
MURI - FY00  
A COMPREHENSIVE APPROACH TO PHONON CONTROL  
FOR ENHANCED DEVICE PERFORMANCE  
5a. CONTRACT NUMBER F49620-00-1-0328  
5b. GRANT NUMBER  
5c. PROGRAM ELEMENT NUMBER

6. AUTHOR(S)  
Merlin, Roberto, D., Project Director  
Principal Investigators: Bhattacharya, P. K.; Goldman, R. S.; Haddad, G; Khurgin, J; Kim, K. W.; Kurdak, C.; Msall, M.; Morkoc, H.; Wang, K.  
5d. PROJECT NUMBER  
5e. TASK NUMBER  
5f. WORK UNIT NUMBER

7. PERFORMING ORGANIZATION NAME(S) AND ADDRESS(ES)  
The Regents of The University of Michigan  
3014 Fleming, Ann Arbor, MI 48109-1340  
8. PERFORMING ORGANIZATION REPORT NUMBER

9. SPONSORING/MONITORING AGENCY NAME(S) AND ADDRESS(ES)  
Air Force Office of Scientific Research  
875 North Randolph Street, Suite 325, Room 3112  
Arlington, VA 22203-1768  
10. SPONSOR/MONITOR'S ACRONYM(S)  
11 AFRL-SR-AR-TR-06-0315

*Dr Matsuura/NE*

12. DISTRIBUTION/AVAILABILITY STATEMENT  
*Distribution Statement A: unlimited*

13. SUPPLEMENTARY NOTES

14. ABSTRACT  
The goals of this program were to identify, develop and implement configurations in which phonons and the coupling of phonons to carriers lead to enhanced device performance. A significant component of our efforts centered on artificial semiconductor heterostructures such as quantum-wells, quantum-dots and superlattices. We considered existing devices such as quantum-heterostructure lasers and detectors and field-effect transistors as well as new concepts relying on the interaction between carriers and coherent phonons, specifically phonon-assisted lasing and tunneling. Highlights of this program include (i) the development of novel theoretical and experimental (ultrafast laser and x-ray) methods to generate and probe coherent high-frequency sound, optical phonons and polaritons, (ii) the improvement of phonon-based imaging techniques and development of new methods of phonon detection, (iii) the demonstration of high-performance quantum-dot lasers, and (iv) the optimization of and development of new epitaxial techniques for nitride growth.

15. SUBJECT TERMS  
coherent phonons, polaritons, ultrafast techniques, x-ray scattering, phonon generation and detection, phonon imaging, nonlinear sound propagation, quantum-dot lasers, tunnel injectors, TUNNET, Si-LED, MBE growth, III-V, nitrides.

16. SECURITY CLASSIFICATION OF:  
a. REPORT b. ABSTRACT c. THIS PAGE  
17. LIMITATION OF ABSTRACT  
18. NUMBER OF PAGES 37  
19a. NAME OF RESPONSIBLE PERSON Roberto D. Merlin  
19b. TELEPHONE NUMBER (Include area code) 734-763-9759

20060727336

# FINAL REPORT

## A COMPREHENSIVE APPROACH TO PHONON CONTROL FOR ENHANCED DEVICE PERFORMANCE

PERIOD: JULY 15, 2000 – DECEMBER 31, 2005

Air Force Office of Scientific Research  
Multidisciplinary University Research Initiative

Award Number: F49620-00-1-0328



### Project Director

Roberto Merlin, Professor  
Department of Physics, University of Michigan, Ann Arbor, MI 48109-1120

### Co-Principal Investigators

Pallab Bhattacharya, James R. Mellor Professor  
Department of Electrical Engineering and Computer Science, University of Michigan

Rachel Goldman, Associate Professor  
Department of Materials Science and Engineering, University of Michigan

George Haddad, Robert J. Hiller Professor  
Department of Electrical Engineering and Computer Science, University of Michigan

Jacob Khurgin, Professor  
Department of Electrical and Computer Engineering, Johns Hopkins University

Ki Wook Kim, Professor  
Department of Electrical and Computer Engineering, North Carolina State University

Cagliyan Kurdak, Associate Professor  
Department of Physics, University of Michigan

Madeleine Msall, Associate Professor  
Department of Physics, Bowdoin College

Hadis Morkoç, Founders Professor  
Department of Electrical Engineering, Virginia Commonwealth University

Theodore Norris, Professor  
Department of Electrical Engineering and Computer Science, University of Michigan

Kang Wang, Professor  
Department of Electrical Engineering, University of California at Los Angeles



## 1. PROGRAM OBJECTIVES

The goals of this program were to identify, develop and implement configurations in which phonons and the coupling of phonons to carriers lead to enhanced device performance. A significant component of our efforts centered on artificial semiconductor heterostructures such as quantum-wells (QW), -dots (QD) and superlattices (SL's). Unlike bulk materials, the phonon properties of these low-dimensional systems and, in particular, the phonon frequency, group-velocity, density of states as well as the strength of the interaction with carriers can be widely modified to improve the performance of devices. In this program, we considered existing devices such as quantum-heterostructure lasers and detectors and field-effect transistors (FET's) as well as new concepts relying on the interaction between carriers and coherent phonons, specifically phonon-assisted lasing and tunneling. Our interactive theoretical and experimental efforts focused on (i) the development of models to predict and guide the experimental search for optimal design and performance of various electrical and optoelectronic devices, particularly for control of thermalization rates, (ii) the improvement of existing and the realization of new coherent optical and acoustic phonon sources using both ultrafast lasers and electrical methods, and (iii) the application and improvement of state-of-the-art materials growth and micro-fabrication methods to implement new ideas for control of phonon parameters, and to develop phonon filters, lenses and reflectors.

## 2. PROGRAM ACCOMPLISHMENTS

### 2.1 Phonon Generation and Detection

#### 2.1.1 COHERENT PHONON-POLARITONS, ACOUSTIC AND OPTICAL PHONONS

**Phonon-Polaritons** - Merlin and co-workers used an optical method based on subpicosecond pulses moving in a nonlinear medium to generate Cherenkov radiation (CR) in the infrared range through phonon-assisted phase matching. The pulses, of central frequency  $\omega_L$ , move through the medium with velocity  $v = c_g(\omega_L)$  and interact with themselves to generate a low-frequency polarization through frequency-difference generation, a nonlinear effect associated with the susceptibility tensor  $\chi^{(2)}$ ;  $c_g = d\omega_L/dq$  and  $q$  are the light group velocity and wavevector. The generation of CR by such methods was pioneered by Auston and coworkers [1] who applied the technique to LiTaO<sub>3</sub> in a range for which  $v \gg c_0$ , where  $c_0$  is the speed of light at zero frequency. In our experiments on ZnTe and ZnSe, we detected emission at subluminal speeds involving frequencies below those of the corresponding infrared-active phonon. Results for ZnSe were reported in [2]. Data for ZnTe is shown in Fig. 1. Compared with conventional ultrafast methods for the generation of coherent THz radiation, our approach shows some advantages on how to attain phase-matching conditions. The generation of Cherenkov radiation by electric dipoles generated by subpicosecond pulses is physically indistinguishable from the excitation of coherent polaritons by impulsive stimulated Raman scattering (RS) [2].

**Acoustic Modes** - Bucksbaum and Merlin [3] proposed that control of coherent phonons can be applied to slice a beam of hard x-rays to generate subpicosecond pulses. This so-called Bragg switch was central to the collaborative effort based at the ANL Advanced Photon Source involving MURI researchers and colleagues at the University of Michigan and other institutions. These efforts led to novel ideas for the development of ultrafast x-ray methods, as well as real-time studies of the propagation of a high-frequency sound pulse across a solid [4]. Figure 2 shows the time-resolved transmission for sound generated by ultrafast laser-excitation at  $t = 0$  on the exit face of a Ge crystal. We detected both the forward and deflected x-rays as a function of time and crystal angle. The x-rays propagate via the Borrmann effect. Starting at  $t = 0$  the diffracted intensity switches from the forward beam to the deflected beam in time whose measurement is limited by

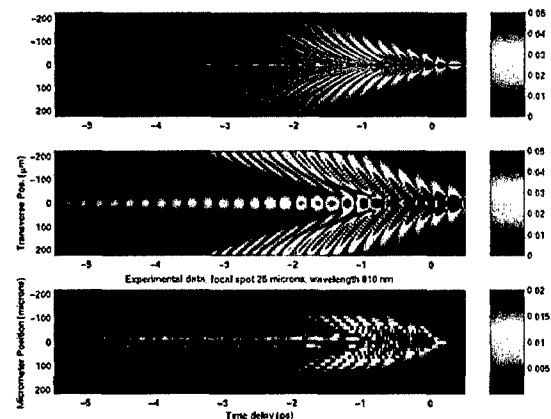


Fig. 1 - Theoretical and experimental plots for ZnTe. (a) Calculated  $E$  vs.  $\rho$  and  $(z/v-t)$  for a point dipole moving at  $v \sim 0.984c_0$ . (b) Convolution of (a) with a Gaussian function. (c) Differential transmission measurements as a function of the probe beam location. For both beams, the central energy and the width of the pulses were 1.53 eV and  $\sim 50$  fs.

the x-ray pulse duration ( $\sim 100$ ps). Approximately 75% of the energy is transferred from one beam to the other. Following the initial switch, Pendellösung oscillations are apparent in both the forward and deflected beams. The oscillations appear to be  $\pi$  out of phase with a frequency of  $\sim 1$  GHz, and they decay over several x-ray attenuation lengths. Around 60ns the acoustic pulse approaches the input face of the crystal at the sound speed, so that the acoustic disturbance forms a thin interface separating the near-input region from the rest of the crystal. This has a large effect on the coupling of the input beam into the  $\alpha$  mode that can cross the thick crystal with relatively little attenuation. As a result, more than 50% of the input intensity couples to the  $\alpha$  wave.

Superlattices of a tailored periodicity provide a means to couple high-frequency sound to light pulses. As opposed to picosecond ultrasonics [5], where the generated acoustic wave has a broad frequency-spectrum and is usually limited to a few hundreds of GHz, superlattices can act as sources of monochromatic acoustic waves of THz frequencies. Although folded acoustic phonons were discovered nearly twenty years ago, there has been renewed interest due to the observation of coherently generated acoustic phonons. Merlin's group developed a model for understanding the dynamics of the high frequency modes in layered structures and superlattices. The model was tested by performing pump-probe ultra-fast optical experiments on samples of AlAs-GaAs based superlattices. They also developed an understanding of the behavior of the modes near surfaces, and related these modes to surface avoiding modes.

Figure 3 illustrates the behavior of a surface-avoiding mode. Calculations of the normal modes show that their amplitude is a maximum inside the superlattice and decreases towards the surfaces. A stationary wave cannot satisfy the boundary condition. Since the solutions are linearly independent at the zone center (and edge), the only way to fulfill the condition is to avoid the surface by making the amplitude of the wave close to zero in its vicinity. Such modes are known as surface avoiding modes.

Time-domain experiments were performed on a superlattice, grown by molecular beam epitaxy, of 75 periods of 59 Å GaAs and 23.5 Å AlAs. A 70 nm layer of AlAs was grown between the superlattice and the substrate to act as an etch stop. The time-resolved experiments were carried out in the standard pump and probe configuration, using an optical parametric amplifier which delivered ultrafast pulses (70 fs) at a rate of 250 KHz tunable in the visible range

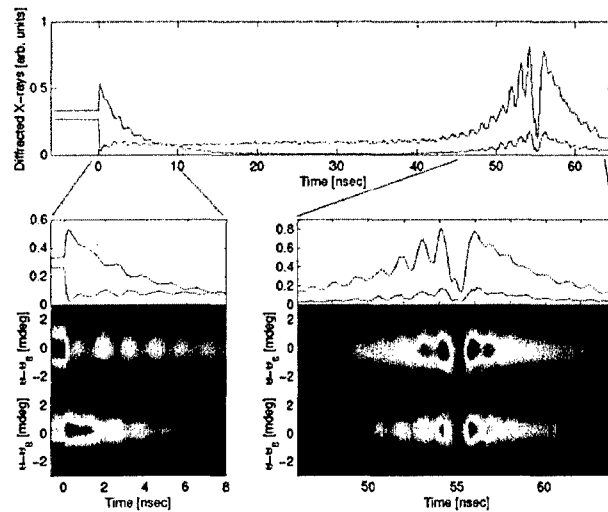


Fig. 2 - Time-resolved diffraction reflection following laser impulsive excitation of an acoustic wave on the exit face of a thick Ge [001] crystal. Top: Forward (blue) and deflected (red) x-ray intensity as a function of time following excitation. Bottom: expanded scale showing the regions where the acoustic pulse is near the exit or entrance crystal surface. 2-d plots: x-ray transmission vs. time and crystal angle near the forward (top) and deflected (bottom) diffraction peaks.

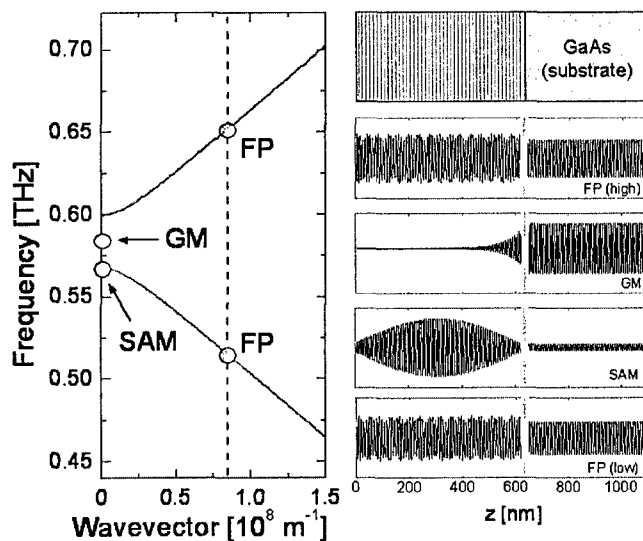


Fig. 3 - Calculated dispersion of LA modes propagating along [001] for the GaAs-AlAs SL investigated in this work. Panels on the right show a schematic diagram and four representative eigenmodes of the 619-nm-thick SL slab (striped area) attached to a 5- $\mu$ m-thick substrate. Vertical green bars denote the SL-substrate boundary. SAM is the surface-avoiding mode at  $q \approx 0$ . The wavevector associated with modes labeled FP is sufficiently far removed from the zone center so that the FP-waves reflect only weakly at the boundary. The mode with frequency in the minigap, GM, decays exponentially into the SL.

(400-650 nm) with a pulse energy of 1 nJ. These pulses are split into pump and probe. The pump excites coherent vibrations of the lattice that modulate the index of refraction and, hence, the reflectivity of a time-delayed probe pulse. The pulses' central wavelength is tuned for resonant excitation with the superlattice at 530 nm. The pump beam is chopped at 2 KHz and the signal is analyzed with a lock-in amplifier at this frequency. All the experiments were done at room temperature. In Fig. 4 we show the differential reflectivity data as a function of the probe time delay between 0 and 250 ps after subtracting a slowly varying background. Similar scans were taken up to 500 ps time delay. An oscillation with a period of 14 ps can be seen and, superimposed, higher frequency oscillations as shown in the inset. Note that what may appear to be noise is actually the superposition of modes of different frequencies. The Fourier transform shows clear peaks even after time delays of 800 ps. The fast Fourier transform of the time trace in Fig. 4 is shown in Fig. 5 together with the dispersion relation shown in Fig. 3. Four peaks can clearly be seen in the power spectrum. By studying the Fourier transform of different time sections we can obtain information on the evolution of the four different modes. In Fig. 5 we show the Fourier transform of time scans similar to the one shown in Fig. 4 for four different time intervals. At short times, four peaks are seen. Here, the triplet near 0.6 THz consists of two peaks corresponding to the modes for  $q = 2\pi/\lambda$  and a peak slightly shifted from the center of the other two that corresponds to one of the modes at the center of the mini-Brillouin zone. As we move to long times, spectra (b) and (c), the doublet (peaks 2 and 4) fades away and only the mode at  $q = 0$  remains visible in

**Optical Phonons** - While there has been widespread agreement that stimulated RS is the key generation mechanism for coherent phonons in the transparent region, its role in opaque materials has remained controversial. Merlin and co-workers demonstrated a previously unrecognized feature of RS that settles the discussion [6]. Specifically, they proved that stimulated RS is defined not by one, but by two distinct tensors. The first one is the standard Raman susceptibility discussed in textbooks which gives both the modulation of the linear susceptibility by the phonon and the cross section for spontaneous RS. The second, new tensor, characterizes the electrostrictive force acting on the ions. Consistent with the common understanding of stimulated Raman processes, the real parts of these tensors are identical and, thus, they become one and the same in the domain of transparency. Relevant to the absorbing region, however, their imaginary components differ appreciably.

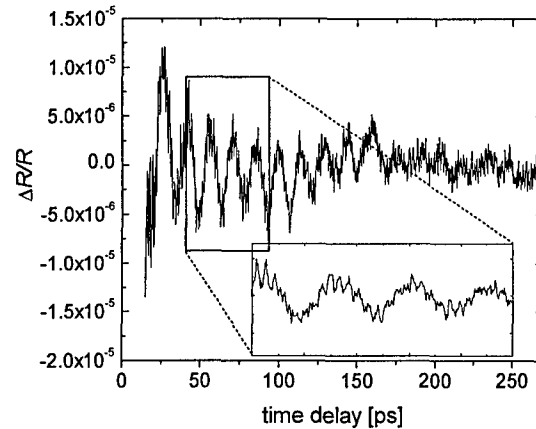


Fig. 4 - Differential reflectivity as a function of time delay.

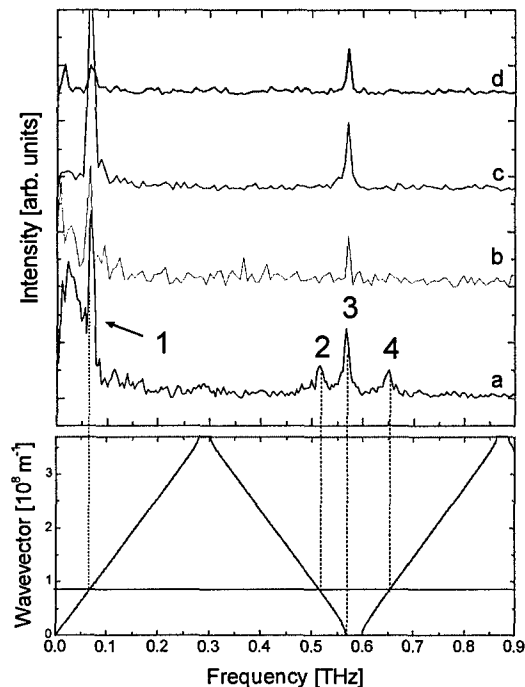


Fig. 5 - Fourier transform of different time sections like the one shown in Fig. 4 together with the dispersion relation calculated with the parameters of the sample. The spectra correspond to, a = 0-125 ps, b = 125-250 ps, c = 250-350 ps and d = 350-500 ps.

These predictions were tested by examining the behavior of coherent phonons generated at photon energies in the range of the  $E_2$  critical point of Sb. The experimental results are in very good agreement with the two-tensor model.

The anharmonic properties of the low-frequency  $E_2$  phonon in ZnO were measured by Merlin and co-workers using impulsive stimulated RS [7]. At 5 K, the frequency and lifetime are  $(2.9789 \pm 0.0002)$  THz and  $(211 \pm 7)$  ps. The unusually long lifetime and the high accuracy in the determination of the frequency hold promise for applications in metrology and materials characterization. The temperature dependence of the lifetime is determined by two-phonon up-conversion decay contributions, which vanish at zero temperature. Results shown in Fig. 6 suggest that the lifetime is limited by isotopic disorder and that values in the nanosecond range may be achievable in isotopically-pure samples. Everitt's group also investigated coherent optical phonons in bulk ZnO using samples that were thermally treated under forming gas environment (from Cermet, Inc. and Eagle-Picher). Phonon lifetimes can be extracted from impulsive stimulated RS measurements. As seen in Fig. 7, the preliminary measurements at Duke University

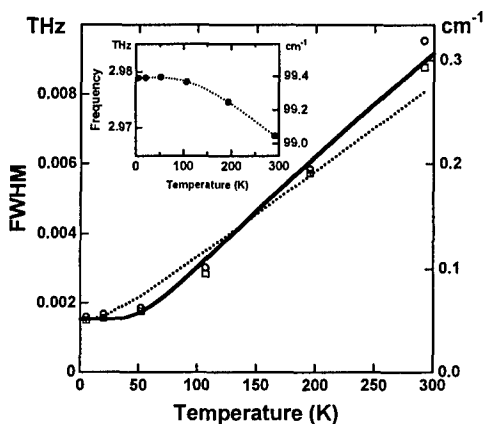


Fig. 6 - Temperature dependence of the Raman-lineshape FWHM from Lorentzian fits to the frequency-domain data (circles) and time-domain fits to the coherent-oscillation amplitude using a simple decaying exponential (squares). Full and dotted lines are fits neglecting, respectively, down- and up-conversion processes. Inset: Frequency vs. temperature. The dotted curve is a guide to the eye.

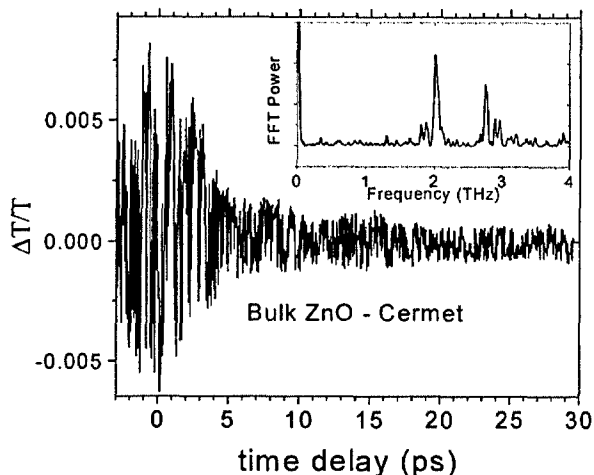


Fig. 7 - Impulsive stimulated Raman data for a bulk ZnO sample (Cermet). The inset shows the fast Fourier transform of the data.

using a mode locked Ti:Sapphire laser at 800 nm with  $\sim 100$  fs pulses show a reasonable ISRS signal at room temperature. The inset shows the fast Fourier transform of the data, which has two well defined peaks at  $\sim 2.05$  and  $\sim 2.75$  THz. Lee *et al.* [8] identified the  $A_1(\text{LO})$ ,  $E_2$ -high, and  $E_2$ -low optical phonon mode frequencies as 17.2, 13.2, and 2.98 THz, respectively, for a hydrothermally-grown bulk ZnO sample. For the observation of  $E_2$ -high, and  $E_2$ -low modes, pump and the probe beams need to be orthogonal; however, the  $A_1(\text{LO})$  mode may be observed in any geometry. In these measurements, the pulse-width of  $\sim 100$ fs limited the observation of any modes with frequencies above 10 THz. The observed frequency of 2.75 THz is very close to the value reported for the  $E_2$ -low mode by Lee *et al.* The dephasing time at room temperature is less than 10 ps.

**Acoustic Modes in Quantum Dots** - Studies of acoustic modes in nanoparticles were pursued in Merlin's group [9]. Using ultrafast optical pulses, coherent phonons were generated in a semiconductor doped glass, made of semiconductor inclusions of nanometer size in an insulating matrix. By tuning the laser to resonate with the absorption edge of the semiconductor QDs, they were able to generate high amplitude coherent optical and acoustic phonons. The stimulated RS model reproduces accurately the experimental results as to be the mechanism responsible for the phonon generation in the absorbing regime. These studies showed that the initial phase of the coherent field carries information about coupling between modes. If the modes are coupled, the initial phase reflects this effect by a phase-shift respect to the phase predicted for independent oscillators. They experimentally detected this phase-shift, due to the coupling between two optical modes, in the time-domain measurements. At low power excitation, they observed that the frequency of the optical coherent phonons deviates from values obtained from spontaneous Raman scattering, as shown in Fig. 8. This effect was ascribed to the presence of electronic impurity states (traps) which modify

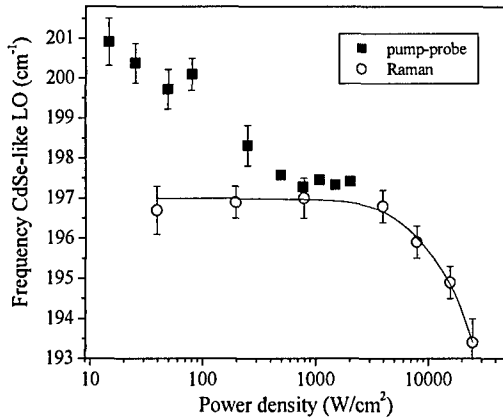


Fig. 8 – Power dependence of the frequency of the CdSe-like LO phonon for Raman and pump-probe measurements.

the nanocrystal dielectric function in the infrared and, thereby, renormalizes the frequency of the optical modes; see the energy level diagram in Fig. 9(left). In particular, a filled electronic trap with an allowed transition frequency larger than the bare optical phonon frequency, will push the effective optical phonon frequency detected to lower values. This happens for all the power densities used in the cw experiment, for which the trap is always full. In time-domain experiments, this effect operates only if the trap filling time is smaller than the phonon time decay, as  $t_1 < \tau_{ph}$  in Figure 9 (right), which correspond to power  $P_1$  ( $n_{0d}$  is the population of the trap level  $0_d$ ). If the power density is always higher than the power to saturate the trap,  $P_0$ , it was shown that moving the power density in time domain experiments, it is possible to go from the renormalized frequency (at power  $P_1$ ) to the bare frequency (at power  $P_2$ ), which is consistent with the behavior seen in Fig. 8.

### 2.1.2 ACOUSTIC PHONONS IN THE NITRIDE SYSTEM

The immense potential of acousto-optical devices based on nitrides as well as the poorly understood physics of acoustic phonons in multiple quantum wells (MQWs) make the study of acoustic phonons particularly important. The collaboration between the groups of Hadis Morkoç at Virginia Commonwealth University, and Henry Everitt, at Duke University, focused on the generation of coherent acoustic phonons in nitride superlattices. Using sub-picosecond optical pump-probe techniques, Everitt and coworkers were able to generate and control coherent zone-folded longitudinal acoustic phonons (ZFLAPs) in InGaN multiple QW structures [10]. Using differential transmission (DT) techniques, their measurements revealed that carriers injected near the barrier band edge were quickly captured into the quantum wells and generated strong coherent ZFLAP oscillations of frequency 0.69 THz. Two-pump DT was used to generate coherent ZFLAP oscillations whose relative timing and amplitude could be controlled. Enhancement and suppression of ZFLAP oscillations were demonstrated. The ability to generate and control acoustic phonons, dramatically simplified by the properties of the InGaN MQW system, is of scientific and technological utility. By canceling coherent ZFLAPs one half period after their creation, a single mode acoustic phonon impulse is generated which can propagate through the sample and whose subsequent effects on the material response can be monitored. It should be possible to probe the effects of single mode acoustic phonon interactions with carriers or excitons in a controlled manner. More generally, complex temporal pump pulse waveforms, created by genetic learning algorithms and spatial light modulators, can be used to create non-trivial phonon excitations to explore or control phonon-mediated decay or dephasing. In addition, spectrally pure, coherent 0.10 THz bulk and 0.69 THz zone folded acoustic phonons were generated using similar impulsive techniques. As before, a single, high frequency acoustic phonon mode was excited using impulsive differential transmission, and it was found that these zone folded acoustic phonons are insensitive to temperature changes between 80K and 300K. Acoustic modes at both frequencies were simultaneously excited using impulsive differential reflection. It was observed that the bulk phonons travel ballistically through the cap layer and reflect efficiently from the semiconductor/air interface, whereas reflected zone-folded phonons were not observed.

Since the coherent acoustic phonon generation is directly linked to the carrier dynamics, it was important to understand the relaxation pathways including carrier capture and recombination. Recent measurements of ultrafast dynam-

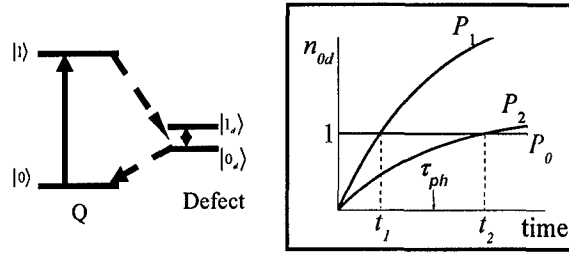


Fig. 9 – (left) Energy diagram of the QD with a single defect. (right) Time dependence of the population of the lowest level.

ics in InGaN and AlGaIn/GaN MQWs helped to identify different processes from sub-picosecond to nanosecond timescales [11]. Carrier capture into the QWs is observed to occur in less than 1 ps and this resulted in an immediate relief of the strain used to generate coherent acoustic phonons.

Another important objective of the Morkoç-Everitt collaboration was to build an acoustic phonon resonator with a frequency of  $\sim 1$  THz. To make this achievable, the coherence time of the acoustic phonons needed to be increased and the leakage from the MQW region had to be minimized. For this reason, AlN/GaN MQW layers were grown by plasma assisted MBE to be used as phonon mirrors on both sides of an InGaN MQW structure. The QW periods were determined from high-resolution x-ray measurements. The superlattice satellite peaks indicate a periodic structure with smooth interfaces.

For acoustic phonon generation, InGaN MQW structures were grown by MOCVD on *c*-plane sapphire substrates with  $\sim 3 \mu\text{m}$  GaN:Si ( $10^{18} \text{ cm}^{-3}$  doping) template layers. Three samples (CVD58, CVD59, CVD75) with 10 periods of  $\text{In}_{0.03}\text{GaN}/\text{In}_{0.15}\text{GaN}$  were characterized by x-ray diffraction, photoluminescence (PL), PL excitation (PLE), and absorption measurements. One of the samples (CVD75) was capped with a  $\sim 50$  nm GaN layer. PL, PLE, and absorption data are shown in Fig. 11. All three samples exhibited intense luminescence. However, the barrier absorption, which was shown previously to be effective in acoustic phonon generation, is low. This explains why time-resolved pump/probe (differential transmission) measurements did not show any sign of acoustic phonon generation. Research is still underway to optimize the growth conditions of the InGaN MQWs to increase the barrier absorption and to obtain better interfaces. These MQW structures will be grown on GaN templates with SiN nanonet and/or AlN/GaN superlattice structures to reduce the defect density in the MQW region. After the InGaN MQW quality is optimized, same structures will be grown on AlN/GaN MQW phonon mirrors.

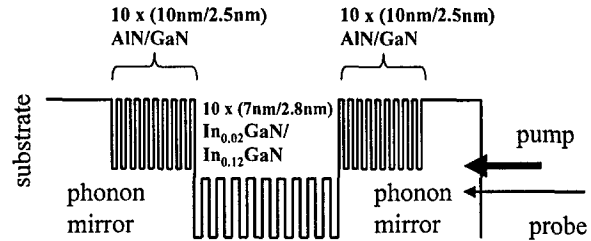


Fig. 10 - Proposed sample structure to increase the confinement of coherent acoustic phonons in the InGaN MQW.

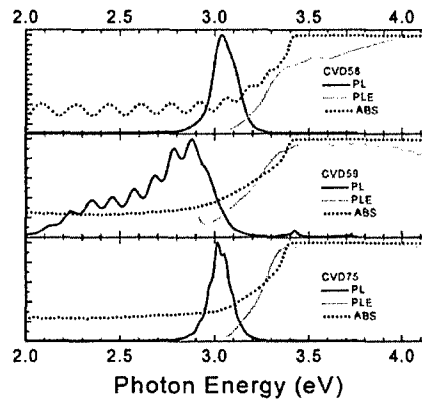


Fig. 11- PL, PLE, and absorption (ABS) data for three InGaN MQW samples.

### 2.1.3 ELECTRICAL GENERATION AND AMPLIFICATION OF COHERENT PHONONS

**Phonon Generation in Nanoscale Structures Under the Overshoot Transport Regime** -- Kim's group analyzed the interaction of high-speed electrons and polar optical phonons in nanoscale semiconductor structures. Under the velocity overshoot regime, it is found that electrons can induce optical phonon instability; i.e., the lattice optical vibrations grow in time when the electric current exceeds a threshold value. For nanoscale diodes based on III-V compounds, the threshold current density is estimated to be of the order of hundred  $\text{kA}/\text{cm}^2$  and the corresponding bias 0.5–1.5 V for the diode lengths of 50–100 nm; see Fig. 12. The wavelengths of unstable phonons are approximately 10 nm with the characteristic time for instability development in the 10 ps range.

**THz Microwave Emission in Ballistic Structures Under Optical Phonon Generation** - In nanostructures with the ballistic electron transport, we found the frequency windows with negative dynamic resistance due to the effect of generation of optical phonons. These windows are near the optical phonon frequency. Kim's group calculated the impedance of the ballistic devices and established that the device can be used for generation of THz emission. The typical parameters obtained for the devices based on III-V compounds are: the device length of about 50-70 nm, the electric bias of 0.1-0.2 V, and the frequencies of 7-8 THz. The low temperature is assumed for ballistic transport.

**Generation of High-Frequency Acoustic Phonons by ac Fields in Acoustic Resonators** - Kim's group proposed and analyzed generation of THz acoustic phonon pulses by using the ac (MHz range) electric field. The device under consideration is a  $n^+(3D)-n(2D)-n^+(3D)$  or a  $p^+-p-p^+$  diode. The base of the diode consists of a heterostructure with

a single or multiple quantum wells, which confine both electrons and phonons. The lateral transport in the base with 2DEG provides amplification of a pulse (packet) of the THz phonons. The pulse moves back and forth reflected at the surfaces of the diode. Generation of the THz phonons arises, when the ac electric field is synchronized with the phonon pulse motion. For example, the generator utilizing a p-doped SiGe heterostructure with the base length of 50.100  $\mu\text{m}$ , can generate pulses of acoustic phonons in the 0.3-0.4 THz range by using the electric fields of 0.5-1 kV/cm with the ac frequency of 20-50 MHz.

#### Light Modulation by High-Frequency Phonons -

Using a photoelasticity model, we studied light modulation by coherent optical phonons generated in AlGaAs/GaAs superlattices. For the case of a plane wave case, the amplitude of the scattered light wave was estimated to be approx.  $10^{-4}$  to  $10^{-3}$  of the incident amplitude. A further analysis demonstrated that the efficiency of light modulation can be enhanced drastically if the phonon generator is placed inside a light cavity. In this case of high-Q Fabry-Perot cavity, the amplitude of the scattered wave can be comparable to that of the incident wave. This suggests that the phonon generators combined with the optical cavity can be used for very efficient cw THz modulation of light, which is not available at present by other means.

This suggests that the phonon generators combined with the optical cavity can be used for very efficient cw THz modulation of light, which is not available at present by other means.

**Phonon Generation by Carrier Drift and Cherenkov Emission-** Kim and collaborators developed a model for the amplification of confined vibrational modes by the drift of the two-dimensional carriers as a function of phonon frequency, temperature and heterostructure parameters. Two electron-phonon interaction mechanisms were taken into account involving interaction via the deformation potential (p-SiGe/Si and n-AlGaAs/GaAs) and the piezoelectric interaction (n-AlGaAs/GaAs). It was found that an amplification coefficient of the order of hundreds of  $\text{cm}^{-1}$  for the AlGaAs heterostructures and thousands of  $\text{cm}^{-1}$  for the SiGe heterostructures can be obtained in spectrally-separated narrow amplification bands. Amplification of shear vertical waves in the heterostructures grown in the direction of high symmetry (for instance, [001]) is found to be significantly stronger than that predicted by the model of elastically isotropic media. The NCSU team used the Cherenkov generation model to investigate optical phonon amplification by a drifting degenerate electron gas. Extension of the analysis for the degenerate gas is important since this is the case most favorable to meet the generation criteria. The results demonstrate high efficiency of optical phonon generation as well as its significant impact on the electron transport in the generation regime. The possibility of optical phonon avalanche was also investigated. A comparison between the experimental data (provided by Prof. K. Tsen of Arizona State University) and the theoretical calculations shows a good fit across the wavevector range under consideration including the presence and location of the threshold wavevector. This observation clearly indicates that the unusually large optical phonon population obtained in the light scattering measurements is due indeed to Cherenkov amplification of nonequilibrium phonons.

#### 2.1.4 IMAGING NANOSTRUCTURES WITH ACOUSTIC PULSES

Norris' group developed a novel acoustic imaging scheme based on ultrafast optical excitation and detection of high frequency ultrasound (coherent longitudinal phonon pulses). The basic idea of the experiment is illustrated in Fig. 13. The sample is a 0.5 mm Si wafer coated on both sides with thin Al films, one of which is lithographically patterned with 1-micron-width lines and grids. The pump pulse heats the surface of the film which causes a thermal expansion which in turn launches an acoustic strain pulse (coherent longitudinal phonons) into the film and substrate. The single cycle pulse so generated will have a peak frequency and bandwidth both  $\sim 100$  GHz and will be a few picoseconds in duration. The pulse propagates across the 0.5 mm Si wafer at a speed  $v_L$ , equal to the velocity of a longitudinal sound wave in Si (111), until it reaches the Al film on the opposite side. The change in reflectivity caused by the strain pulse can be detected there by a time delayed optical probe pulse derived from the same Ti:sapphire laser as the pump. Since the characteristic diffraction length for a single cycle pulse is given by the ex-

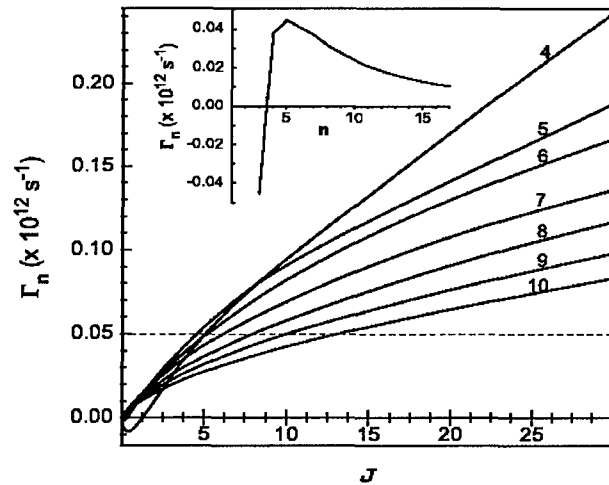


Fig. 12 - Current induced increment  $\Gamma_n$  for different optical modes in a 75-nm long GaAs n-i-n diode in the overshoot transport regime. The current  $J=1$  corresponds to 33 kA/cm<sup>2</sup>. For  $J=20$ , the applied voltage is 0.55 V. The inset shows  $\Gamma_n$  vs the mode number  $n$  at  $J = 4$ . The dashed line indicates the optical phonon loss at  $T = 100$  K.

pression  $z = r_0^2/vt_0$ , where  $v$  is the velocity (9355 m/s) and  $t_0$  is the temporal pulse width ( $\sim 2.5$  ps) they find that for a radius,  $r_0 \sim 3\mu\text{m}$ ,  $z \sim 0.4$  mm which is less than the thickness of the wafer. Therefore, it is possible to probe the picosecond acoustic pulse in the far field regime for a tightly focused pump spot, and the near field regime for a larger pump spot.

It is important to note that in this proof-of-concept experiment, the object to be imaged is actually the source of the detected acoustic waves. The purpose of such a relatively thick sample is to allow the scattered acoustic pulses to propagate a sufficient distance so that variations in the spatial profile of the measured acoustic field can be probed with a diffraction-limited optical probe spot. This long acoustic propagation length requires the sample to be held at cryogenic temperatures in order to suppress the phonon-phonon scattering that strongly attenuates acoustic waves of such high frequency. The changes in reflectivity caused by the propagating phonon pulses are then measured with time-delayed optical probe pulses, giving measurements of the scattered acoustic field. The measured field is then used as the input to a “time-reversed” Huygens-Fresnel diffraction equation in a numerical backpropagation algorithm in order to generate a reconstruction of the Al pattern that launched the waves.

Figs. 14 (a) and 14 (b) show the reconstructed acoustic image of an array of 1 micron lines and an SEM of the same structure, respectively (scale bar on all figures = 5  $\mu\text{m}$ ). To obtain this image, it was necessary to account for the elastic anisotropy of the crystalline Si wafer. The image shown in Fig. 14 (c) is not corrected for this anisotropy effect. It is evident from the figures that the periodicity and shape of the acoustic image was incorrect prior to the use of an anisotropic sound velocity calculated from the known elastic constants of Si.

After establishing the correct backpropagation algorithm for the acoustic imaging scheme, the first 2-D ‘picosecond ultrasonic’ images of nanostructures were obtained [12]. Fig. 14 (d) shows a lineout from the image of Fig. 14 (a), and illustrates that the imaging resolution in these figures is a modest 700 nm, far from the optimum  $\sim 30$  nm resolution that could theoretically be achieved with such high frequency acoustic waves. Future plans include resolution improvement efforts, as well as making the first images of subsurface structures, which will showcase the true advantage of an ultrasonic technique. Related work will include the investigation of different materials as transducer layers, in the hopes of improving fundamental signal-to-noise level in the detection of small acoustic transients.

In addition to imaging with coherent phonons, Norris’ group investigated phonon pulse propagation (dispersion, diffraction, and nonlinearity all must be considered) with a similar experimental arrangement. This work is of interest both from a fundamental standpoint as well as through its usefulness in determining the viability of imaging schemes. The key contribution made through this investigation was to quantify the effects of diffraction on coherent phonon pulses in an anisotropic crystalline medium. Their work in this direction led to a fruitful collaboration with the theoretical group of Jacob Khurgin at Johns Hopkins University.

### 2.1.5 PHONONIC IMAGING OF INTERFACES

Asymmetric interfaces exhibit both mode-conserving and mode-converting scattering. Thus, they display the full potential of tri-refractive acoustic materials. This complexity could be an advantage for phonon optics applications. For example, a well designed asymmetric interface could be used to convert the longitudinal waves normally launched by picosecond excitation of heterostructures to transverse bulk waves. The ability to generate both longitudinal and transverse bulk waves would greatly extend the current range of picosecond ultrasonic experiments.

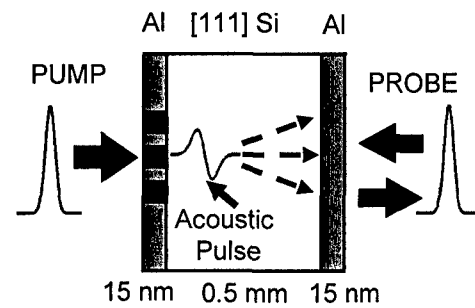


Fig. 13 - Schematic diagram of the experiment.

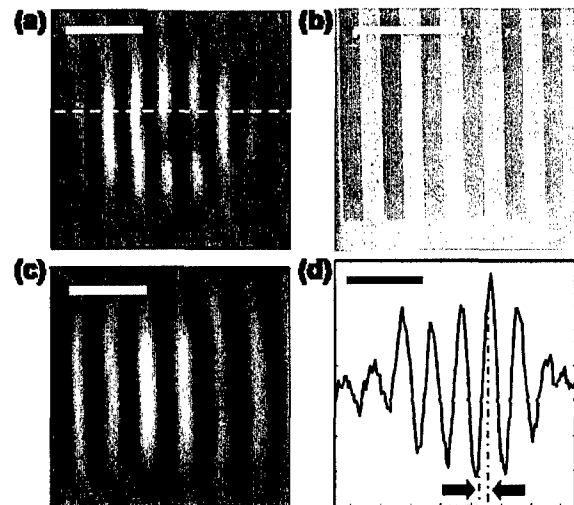


Fig. 14 - Phonon imaging of 1  $\mu\text{m}$  lines.

Msall's work on a grain boundary in  $\text{CaF}_2$  highlights the challenges of creating detailed models of phonon scattering at asymmetric interfaces. High quality modeling of asymmetric interfaces requires extremely accurate structural information available that we obtain using Electron Backscatter Diffractometry (EBSD). Fig. 15 shows the phonon flux pattern for a  $\text{CaF}_2$  sample in which the first section is characterized by Euler angles  $\phi_1 = 2^\circ$ ,  $\theta_1 = 17^\circ$ ,  $\psi_1 = 37^\circ$ , and the second by  $\phi_2 = 57^\circ$ ,  $\theta_2 = 36^\circ$ ,  $\psi_2 = 62^\circ$ . The features in the computer simulation (Fig. 15 (a) and (b)) compare well with those in the experimental image, Fig. 15 (c). There are minor distortions in some feature shapes (e.g., the feature marked  $\delta$ ) because the grain boundary is not perfectly planar, as the computer simulations assume. Of particular interest are regions of high flux intensity in the experimental image that correspond to features identified in the simulations of intermode conversion events (e.g., the right section of the feature marked  $\beta$  and the features marked  $\eta$  and  $\gamma$ ). Most of the highly concentrated flux of this type is due to intermode conversion between the two transverse modes (depicted in purple), but there is also some weakly concentrated flux due to longitudinal to transverse intermode conversion (depicted in green). For these regions, a significant fraction of the energy of a coherent longitudinal wave could be converted into transverse waves. The success of this  $\text{CaF}_2$  project was dependent upon the careful calibration of the BEDS data and required us to develop new local expertise in the use of BEDS for materials analysis. To capitalize on that expertise, we plan to pursue BEDS studies of GaN thin films on a variety of substrates.

Work at Bowdoin on phonon refraction at interfaces involved a variety of systems and, in particular, non-cubic materials such as sapphire-GaN interfaces. New computer routines were developed to simulate both refraction and reflection at these interfaces. The codes are suitably general to handle materials of any symmetry class. As shown in Fig. 16, reflection imaging allows one to probe phonon states without requiring large amounts of material for the transmitted layer. Polarization and frequency dependence of phonon scattering at the interface can be inferred by the characteristics of reflection caustics in the substrate layer alone. Thus, the use of reflected phonon imaging to study phonon states in thin films and low-dimensional structures was of particular interest to the MURI collaboration. Msall's group pursued a series of experiments characterizing the qualities of reflected phonon pulses from a variety of interfaces, including clean sapphire-liquid helium interfaces, wafer-bonded interfaces and epitaxially grown GaN on sapphire (samples from Morkoç). The results emphasize the need for high quality substrates and well-characterized phonon detectors. The expertise gained from single film trials was useful to phonon imaging studies of GaN clusters in a GaAs matrix (using samples provided by Goldman). In this latter case, the structures have characteristic length scales comparable to the dominant phonon wavelengths used to probe them, which promises to provide an interesting glimpse of phonon interactions in very small structures. Two Bowdoin students worked on projects related to the MURI grant. They are, John Koster, a sophomore who worked with the new mask aligner on the fabrication of small scale surface patterns, to be used in studying the effect of surface patterning on phonon reflection, and Elizabeth Robinson, a junior, who worked on the computer simulation of non-cubic interfaces and is considering a senior thesis on phonon reflection imaging experiments. The Msall group at Bowdoin also helped charac-

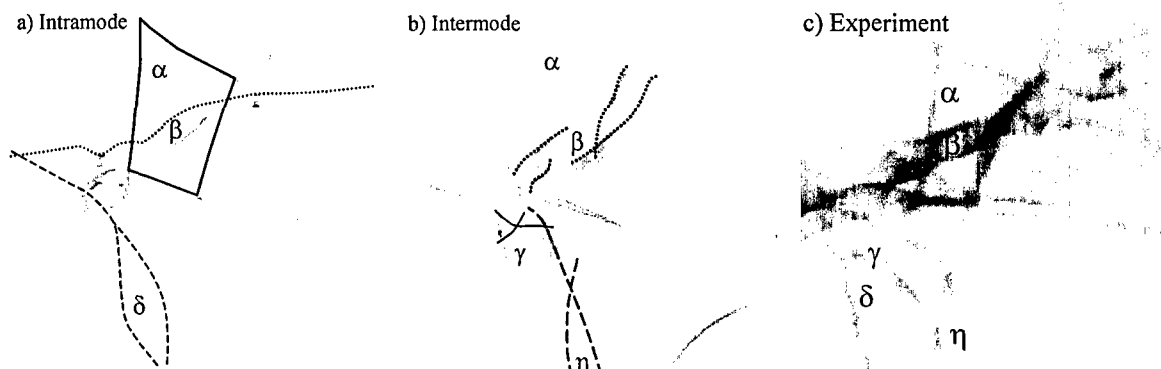


Fig. 15 - Phonon images of  $\text{CaF}_2$  with a grain boundary. Sample thickness = 2 mm, scan range 6 mm x 6 mm. a) Computer simulation limited to mode conserving scattering at interface (FT $\rightarrow$ FT blue, ST $\rightarrow$ ST red, L $\rightarrow$ L yellow); b) Computer simulation limited to mode mode converting scattering (FT $\rightarrow$ ST and ST $\rightarrow$ FT purple, L $\rightarrow$ ST orange, L $\rightarrow$ FT green). c) Experimental image.

terize a novel phonon detector, fabricated by the UM group of Kurdak. The device, described in the next section, makes use of the cyclotron resonance in an extremely long Hall bar to produce a tunable, narrow band detector. The measurement of the response of this device to phonon signals was undertaken with the assistance of Professor Dale Syphers of Bowdoin College, who has many years experience in Quantum Hall measurements. The coordination of his 12 Tesla magnet with optical access and the phonon imaging apparatus was a vital component of these measurements.

### 2.1.6 PHONON DETECTORS

**Hall bars as phonon detectors** - Msall's group observed a very strong interaction between acoustic phonons and a 2D electron gas confined in an AIAs quantum well. The strength of this interaction gives these quantum wells the potential to be a very effective phonon detector. In these experiments, a small AIAs QW structure on one side of a GaAs substrate is used to detect phonons generated in a laser-heated spot on the other side. The AIAs structure is shaped like a cross measuring 30  $\mu\text{m}$  across and has 4 contacts that facilitate both phonon experiments and electric characterisation.

Figure 17(a) shows an image of the phonon induced voltage changes measured between two opposite contacts while scanning the laser spot over an area of about 1.5 x 1.5  $\text{mm}^2$ . Bright and dark areas correspond to positive and negative voltages measured across the AIAs device, respectively. The main features of the image resemble those of the well-known phonon images of an (001)-oriented GaAs crystal. The phonon signal is positive and negative depending on the direction of the wave vector of the absorbed phonons. The size of the phonon signals from this AIAs structure is at least a factor of 10 larger than the signals in comparable GaAs structures [13].

Fig. 17 (b) and (c) show the expected phonon signal based on simulations that include phonon coupling by the piezoelectric interactions and the deformation potential coupling of phonons to the two X-electron valleys, respectively. The experimental results agree well with the deformation potential simulation, particularly the coupling to the slow transverse (ST) modes. The symmetry of the experimental image features also indicates that the valley splitting is negligible on the energy scale of the phonons ( $\approx 1$  meV) of this experiment. The experimental image also shows strong phonon intensities near the center that do not arise from either the deformation potential or the piezoelectric interaction. These features may be a consequence of the detector geometry. Additional simulations that include this factor are planned. The same AIAs structures show very pronounced fractional quantum Hall effects if they are cooled down to temperatures below 100 mK. This makes these quantum wells an attractive alternative to GaAs heterostructures for the phonon studies of the fractional quantum Hall effect.

**Low dimensional electron systems as phonon detectors** - Work in the group of Kurdak focused on the development of tunable phonon detectors based on low-dimensional electron systems. In particular, they have explored using quantum wire and quantum dot devices as phonon detectors. To characterize the quantum wire detectors, Kurdak's group deposited Al on the backside of the GaAs substrate. Phonons were generated by hitting the Al with a short laser pulse. The phonons travel ballistically in GaAs at low temperatures. They were able to detect such ballistic phonons by operating the quantum wire detector with a cryogenic HEMT. Alternatively, on some of the devices, they fabricated electrical heaters on the back side of the GaAs substrate. We have been comparing phonon response of quantum wire detectors for the two cases when the phonons are generated electrically and optically. We find that there are a broad range of time scales involved with the relaxation of electrons excited by phonons in such sensors. The phonons generated by the electrical pulses are typically detected using lock-in techniques. A typical phonon response measurement of the quantum wire device is shown in Figure 18.

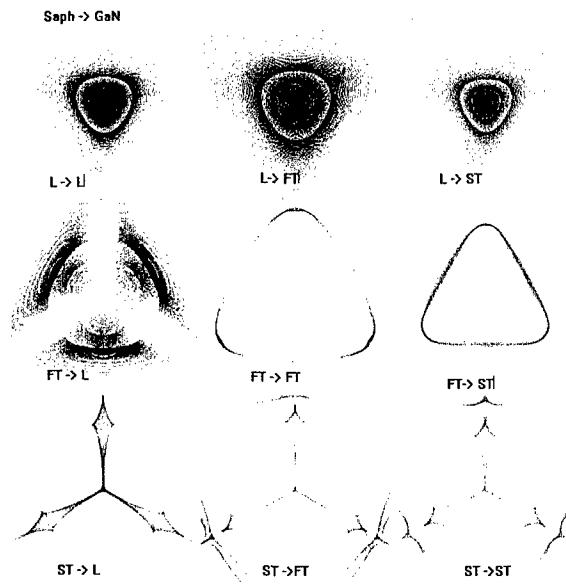


Fig. 16 - Simulated phonon images of GaN on sapphire (substrate and film of equal thickness). The images show the spatial distribution of phonons that have undergone a particular type of mode-conversion at the interface (modes are sorted by velocity and labeled L, ST and FT for longitudinal, slow transverse, and fast transverse). The probability of mode conversion at the interface is determined by requiring continuity of displacement and strain at the boundary. In this figure, all mode conserving and mode converting possibilities are given equal weight.

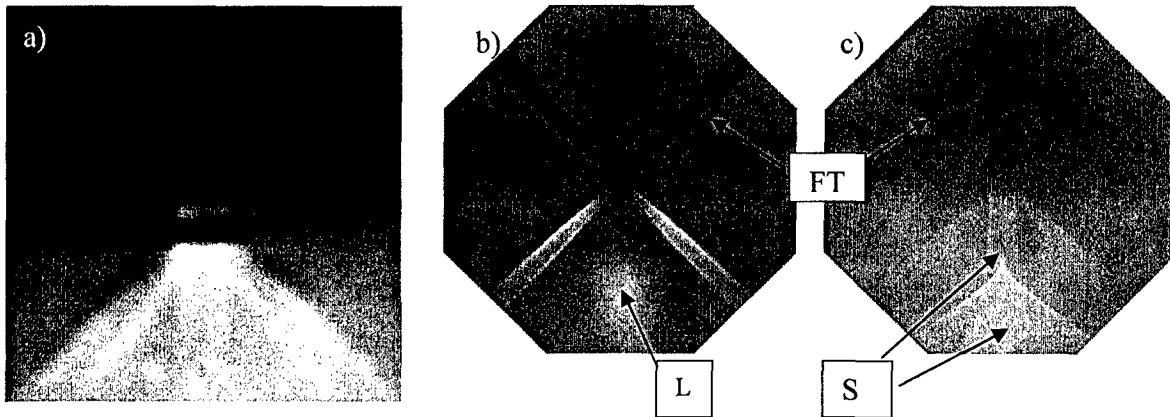


Fig. 17 - (a) Phonon drag image of an AlAs quantum well. The center of the image corresponds to the [001]- direction. The diagonals of both images run along the [100] and [010] planes. The voltage contacts to the 2DEG device are at the top and the bottom, respectively. b) Simulation based on piezoelectric electron-phonon coupling. c) Simulation based on deformation potential electron-phonon coupling.

Quantum dot devices have also been fabricated. Potentially, in addition to being tunable, a quantum dot detector can have enough sensitivity to detect a *single* phonon. To achieve single phonon detection limit, quantum dot detectors must be operated in a dilution refrigerator. A SEM picture of a quantum dot detector is shown in Fig. 19. To perform phonon experiments at dilution refrigerator temperatures, we must generate phonons electrically. Kurdak's groups recent theoretical calculations indicate that the phonon response in such devices are expected to be much larger in hole systems. They are currently fabricating quantum wire and quantum dot sensors using a high quality GaAs/AlGaAs heterostructure with a two-dimensional hole gas.

Kurdak's group has also been exploring the use of double quantum well structures for detecting THz LA phonons. Unlike conventional tunnel devices, the tunnel coupling between two 2DEGs can be very strong when the carrier densities of the layers are identical. This particular feature has been used to realize a novel double quantum well field effect transistor by a group from Sandia National Laboratories. A similar structure has also been used to detect 600 GHz radiation. Collaborations with the Sandia group have begun to investigate the use of the same structures as phonon detectors in the same frequency range. Unlike quantum wire and quantum dot devices such phonon sensors will operate at zero magnetic field. Phonon energy of the sensor will be achieved by controlling the relative Fermi energy of the parallel two-dimensional electron gases using a back gate. They have fabricated such sensor and shown that demonstrated that the Fermi energies can indeed be tuned in the desired range.

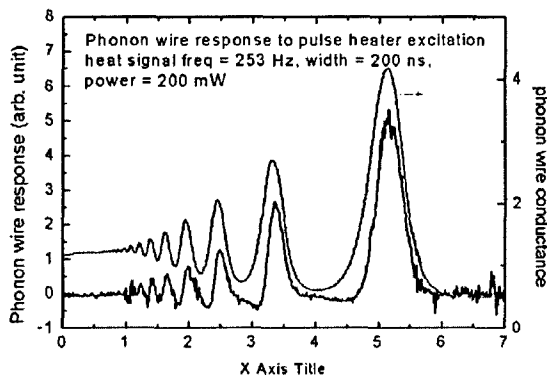


Fig. 18 - Ballistic phonon response of a quantum wire detector.

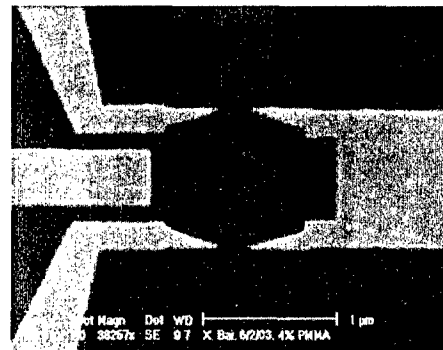


Fig. 19 - SEM picture of a quantum dot detector

## 2.2 Phonon Engineering and Active Control

### 2.2.1 NONLINEAR PROPAGATION OF THz SOUND

Motivated by the experiments conducted by the group of Ted Norris (University of Michigan), Khurgin's group have pursued modeling the nonlinear propagation of acoustic pulses. The experiments involved laser excitation of picosecond acoustic pulses and their propagation in bulk Si. Previously, some soliton-like features had been observed and explained. In the final year of this grant, Khurgin's efforts concentrated on adding diffraction to the picture – they rigorously derived propagation equations that include effects due to nonlinearity, dispersion and diffraction. For the first time the anisotropic diffraction equation was obtained. Using these equations, Khurgin's group successfully modeled the pulse propagation numerically and achieved results that are very close to the experimental ones; see Fig. 20 [14].

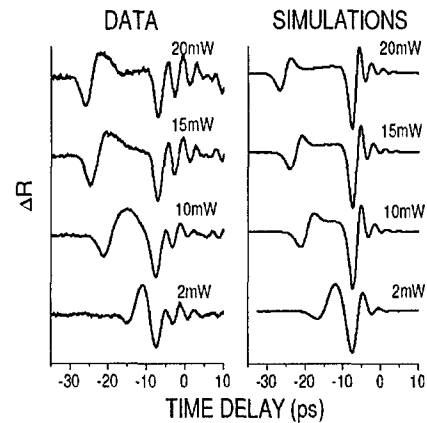


Fig. 20 - Experimental results and simulations for picosecond acoustic pulses experiencing effects of dispersion, diffraction and nonlinearity.

### 2.2.2 OPTICAL PHONONS IN STRUCTURES WITH PERIODICALLY INVERTED POLAR DOMAINS

Khurgin's group completed their work on periodically inverted polar domains –the quasi-phase-matched structures for polar optical phonons (Fig. 21). They calculated the dispersion relations in these structures and derived the interaction Hamiltonians and selection rules for various electronic and optical processes involving phonons in PIPDS – Fröhlich and deformation potential scattering, Raman and infrared. The results shown in Fig. 22 demonstrate that the selection rules are drastically different in PIDPS. These results are reported in [15].

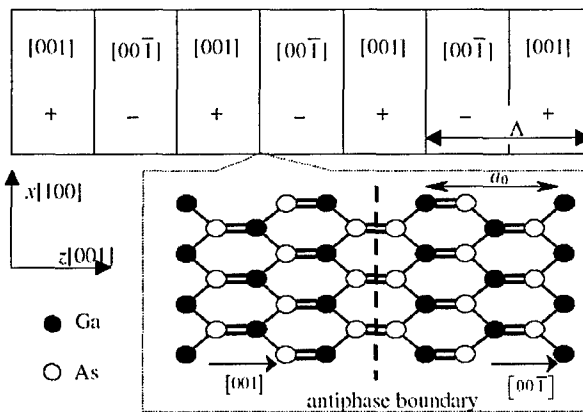


Fig. 21 - Periodically-inverted polar domain structure.

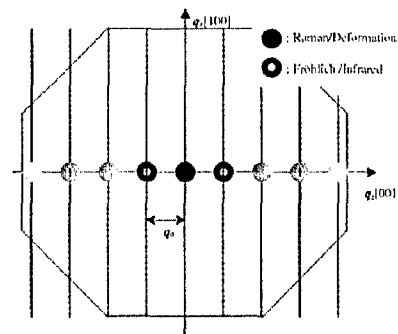


Fig. 22 - Location of scattered optical phonons in the Brillouin zone of a PIPDS structure. The strength of each process is represented by the gray scale.

### 2.2.3. STIMULATED POLARITON SCATTERING IN INHOMOGENEOUSLY BROADENED MEDIA

Khurgin's group pursued work on the new and exciting topic of stimulated intersubband Raman scattering by polaritons. Fig. 23 (a) compares a typical three-level intersubband laser with the Raman intersubband process; see Fig. 23 (b). Whereas they look similar, the re-lasing should always have higher gain than that of a virtual Raman process. However, experiments by the NRC group show that Raman processes dominate – a fact that is difficult to explain. Khurgin and co-workers developed a theory in which the Raman process does not end up in a given one-particle intersubband excitation but results in stimulated emission of quasi-particles consisting of intersubband plasmon, phonon and photon. They show that the gain for such process in inhomogeneously broadened media is stronger than lasing gain due to the effect of motional broadening.

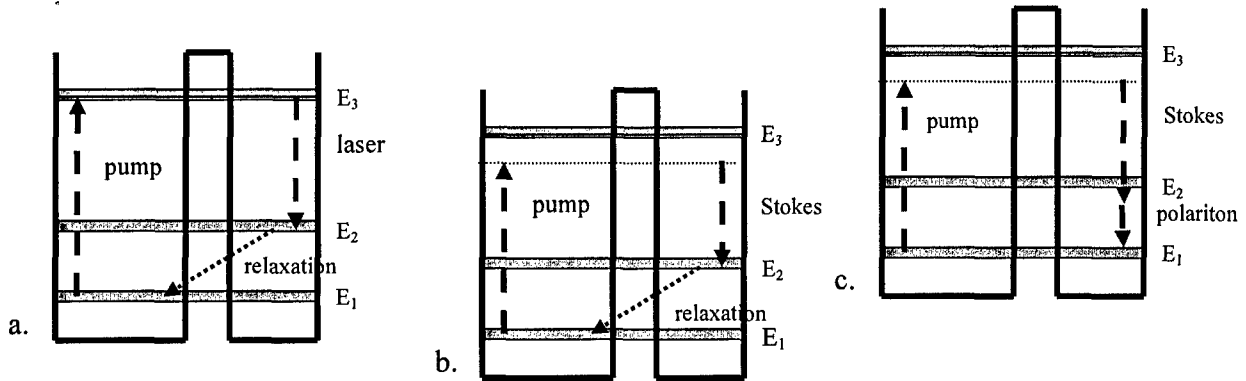


Fig. 23 - Intersubband Processes: (a) lasing, (b) stimulated Raman and (c) stimulated Raman polariton

### 2.2.4 OPTIMIZED PHONON ENGINEERING OF NONLINEAR OPTICAL DEVICES

The group led by Khurgin worked on the design of multiple GaN/AlN QW structures for nonlinear optical devices at communication wavelength (1550 nm). The purpose of this study was to develop and optimize the minimum switching power  $P_w \sim \hbar\omega / \sigma\tau$  where  $\sigma$  is the absorption cross-section and  $\tau$  is the relaxation time at a given bandwidth  $B$ . Intersubband transitions in nitride QWs have large absorption cross-sections ( $> 10^{15} \text{ cm}^{-2}$ ) but the relaxation times are at least an order of magnitude smaller than necessary for, say, 40GBs bandwidth. The relaxation times are determined by LO phonon and piezoelectric scattering. They showed that by using coupled QW's (Fig. 24) one can tailor the relaxation time to the bandwidth to get the best performance.

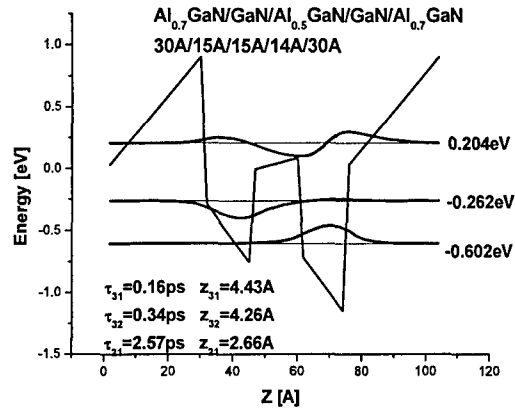


Fig. 24 - QW with phonon-engineered optimal relaxation time.

### 2.2.5 QUANTUM DOT LASERS

Understanding of carrier dynamics and hot-carrier effects in quantum dots and novel design of the carrier injection scheme has led to self-organized QD lasers with performance characteristics comparable to or better than those of QW lasers. Benefiting from the large density of states, quantum dot lasers demonstrate large  $T_0$ , low threshold current, large modulation bandwidth and low chirp. For open-air applications, there is a need for reliable lasers which are also eye-safe. This necessitates operation wavelengths in the range of 1.3-1.55 $\mu\text{m}$ , which is also the range of preference in fiber optical communication systems. While great progress has been made with devices emitting at  $\sim 1\mu\text{m}$ , much less has been achieved with devices emitting at 1.3 and 1.55 $\mu\text{m}$ . Furthermore, there are unique problems that limit the performance of conventional SCH QD lasers, compared to what is expected from "ideal" QD lasers with near singular density of states. Bhattacharya's group proposed the development of high performance quantum dot lasers emitting at 1.3 $\mu\text{m}$ . Specifically, two solutions were proposed to circumvent the inherent unique problems of conventional SCH QD lasers, namely, tunneling injection (TI) and p-doping of the dots. In the following, we summarize the achievements and progresses in 1.3 $\mu\text{m}$  p-doped and tunnel injection lasers.

**1.3 $\mu\text{m}$  p-Doped Quantum Dot Lasers** - The p-doped SCH QD laser heterostructures were grown by MBE on (001) GaAs substrate. Both undoped and p-doped QD lasers were grown and fabricated. In the doped lasers, the modulation doping of the dots was achieved by delta-doping the GaAs barrier/waveguide regions separated from the neighboring quantum dot layer by 14 nm. The doping concentration was varied to provide sheet acceptor concentra-

tion per quantum dot layer varying in the range  $(0-2) \times 10^{12} \text{ cm}^{-2}$ . The optimum doping level was determined by studying the luminescence of the dots and the device characteristics. From the LI characteristics of the broad area lasers of varying cavity length at  $15^\circ\text{C}$ , we determine the value of internal quantum efficiency,  $\eta_i$ , and cavity loss,  $\gamma$ , to be 62% and  $6.6 \text{ cm}^{-1}$ , respectively, for the p-doped samples with an optimized delta-doping of  $5 \times 10^{11} \text{ cm}^{-2}$ . The value of  $J_{th}$  is  $390 \text{ A/cm}^2$  for  $400\mu\text{m}$  cavity length. For the undoped QD lasers,  $\eta_i$ ,  $\gamma$ , and  $J_{th}$  are 0.89,  $4.3 \text{ cm}^{-1}$ , respectively. The threshold current density is about  $155 \text{ A/cm}^2$  for  $400\mu\text{m}$  cavity length, which is less than the p-doped samples. The LI characteristics of a single mode p-doped laser, measured at various temperatures, are shown in Fig. 25(left). Plotted in Fig. 25 (right) are the threshold current and differential efficiency as a function of temperature, as derived from the data of Fig. 25(left). It is evident that  $I_{th}$  is independent of temperature in the range  $5-75^\circ\text{C}$  ( $T_0=\infty$ ) and so is the differential efficiency. *This is the first time that a semiconductor laser has displayed such temperature invariant features.* In contrast, the conventional undoped QD lasers exhibit  $T_0=69\text{K}$  in the same temperature range. We attribute the zero temperature dependence of the p-doped devices to the significant role of Auger recombination in  $1.3\mu\text{m}$  QD lasers, and its decrease with temperature due to the temperature dependence of Auger coefficient.

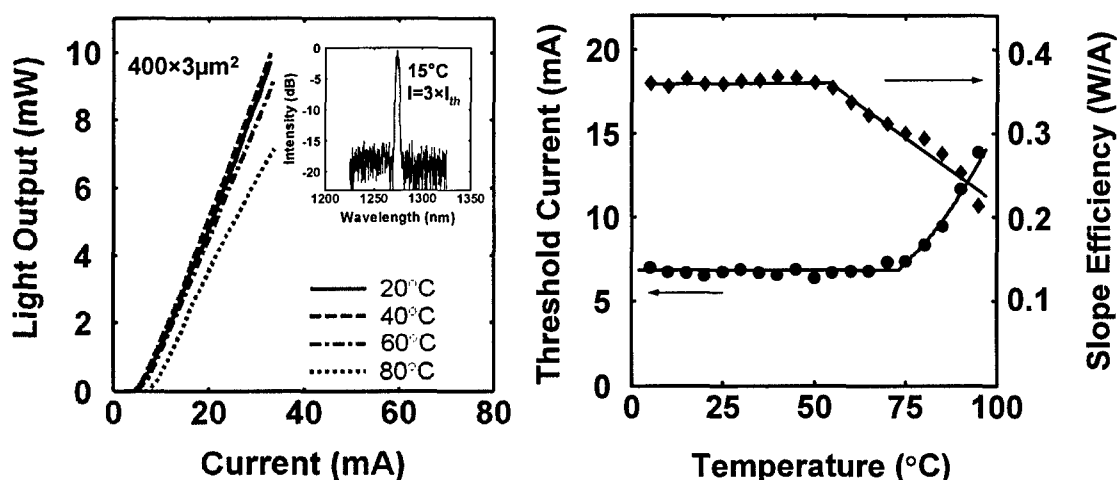


Fig. 25 - Left: Pulsed light-current characteristics of  $1.3\mu\text{m}$  p-doped single mode QD lasers at different temperatures. The inset shows the output spectrum at  $15^\circ\text{C}$ . Right: variation of threshold current and slope efficiency of the lasers with temperature. The lines are fits to the experimental data.

**1.3μm Tunnel Injection Quantum Dot Lasers** - Bhattacharya's group has previously demonstrated high-performance  $1.0\mu\text{m}$  TI QD lasers with  $\sim 25\text{GHz}$  modulation bandwidth, zero linewidth enhancement factor and negligible chirp. This experience has been utilized in design, growth and fabrication of  $1.3\mu\text{m}$  TI QD lasers. The schematic of the designed laser is shown in Fig. 26(a). The active region consists of five layers of capped InAs quantum dots with  $40 \text{ nm}$  buffers in between. Recent calculations of optical phonon assisted transitions in an asymmetric double quantum well heterostructure suggest that tunneling can be more efficient if the populated states of the injector well are energetically aligned with a higher sublevel in the dot. Therefore, unlike our  $1.0\mu\text{m}$  TI laser design where electrons are injected into the ground state of the dots by phonon-assisted tunneling, electrons are injected into the first excited state from a  $9.5\text{nm}$ -thick  $\text{In}_{0.27}\text{Ga}_{0.73}\text{As}$  layer; see Fig. 26(b). This reduces the strain of the epitaxial layers in the  $1.3\mu\text{m}$  heterostructure. The  $1.3 \mu\text{m}$  tunnel injection QD laser heterostructures were grown by MBE on (001) GaAs substrate. Single-mode ridge waveguide lasers ( $3-5\mu\text{m}$  ridge width) were fabricated by standard lithography, wet and dry etching, and metallization techniques.  $200-2000\mu\text{m}$  long lasers were obtained by cleaving. The light-current characteristic of the lasers at  $15^\circ\text{C}$  is presented in Fig. 27. The threshold current is less than  $25\text{mA}$  for  $5\mu\text{m} \times 1500\mu\text{m}$  cavities. The spectrum of the device lasing at about  $1255 \text{ nm}$  is also shown in Fig. 27. Measurement of modulation bandwidth and other dynamic properties of the lasers are currently underway. It is expected that  $1.3\mu\text{m}$  TI QD lasers exhibit  $>15\text{GHz}$  modulation bandwidth, with ultra-low chirp and linewidth enhancement factor, which will be a breakthrough in the performance characteristics of  $1.3\mu\text{m}$  light sources for open-air and other hosts of applications.

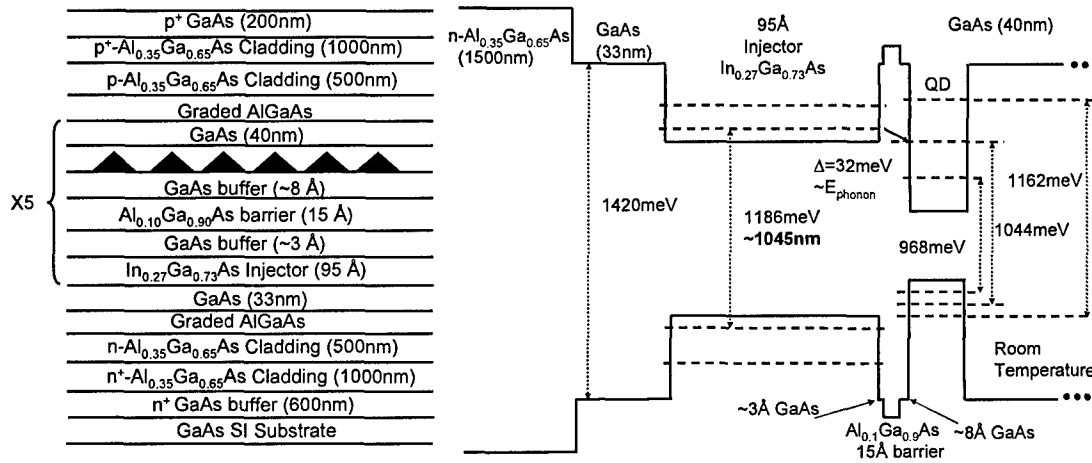


Fig. 26 - (a) The heterostructure of 1.3μm tunnel injection QD laser; (b) Band diagram of the active region, showing tunneling into the first excited states of the dots.

### 2.2.6 PHONON CONTROL FOR ENHANCED PERFORMANCE OF THz SOURCES

The goal of this portion of the project is to investigate transport and injection properties of semiconductor structures in order to realize RF sources that will operate at frequencies between several hundred GHz and several THz. This range corresponds to RF periods between several picoseconds and a fraction of a picosecond. Details of the transport at this time scale are needed to optimize device operation. Transport properties are determined by electron-phonon interactions that are best studied using Monte Carlo techniques instead of techniques that depend on averages over a larger number of scattering events. It is also important to investigate both high mobility materials such as GaAs and wide bandgap materials such as GaN. Finally, we need to study the injection properties of tunneling contacts and the details of ionization on short time scales in order to optimize the device performance. This report will briefly describe the analysis of tunneling injectors for transit time devices, describe the modeling of carrier drift for THz time scales and finally use these results to study device operation at THz frequencies.

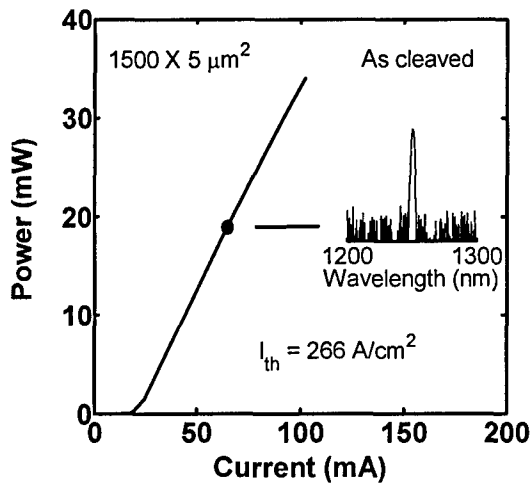


Fig. 27 - Pulsed light-current characteristics of 1.3μm tunnel injection QD lasers at 15°C. The inset shows the output spectrum.

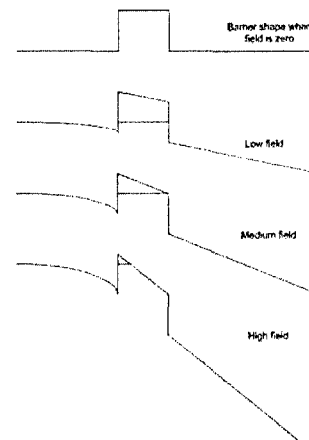


Fig. 28 - Conduction band for biased hetero-junction barrier tunneling injector.

**Tunnel Injectors** - Haddad's group has carried out a detailed study of tunneling injection into semiconductors using heterojunction barriers. The band configurations of the proposed structure are shown in Fig. 28. The zero bias condition is shown at the top with the yellow portion above the contact Fermi level when bias is applied. The barrier changes from nearly rectangular, to triangular with a width equal to the physical barrier width, to a triangular barrier that is much narrower than the physical barrier. The resulting current vs. voltage characteristics for a 100 Å GaAs-AlGaAs barrier are shown in Fig. 29. The injection properties of the barriers are independent of the barrier thickness for all but the very narrow barriers. The transport properties also depend on the barrier height, which in this system depends on the barrier Al fraction. Transport properties for a range of barrier Al fractions are shown in Fig. 30. Although the Al fraction effects the turn on electric field, the junction conductance at a given current density is approximately the same. The modest current densities and conductance of these tunneling barriers limits the THz operation of tunneling based injectors. These limitations will be discussed after first describing the transient transport.

**Monte Carlo Based Investigation of Transient Transport** - The properties of electron transport over small distances and short time scales can be investigated using Monte Carlo techniques. We have modified several Monte Carlo programs obtained with the help of Prof. Umberto Ravaioli of The University of Illinois. Typical calculation results for GaAs are shown in Fig. 31. This figure shows that for time scales on the order of 50 fsecs injected electrons are moving nearly an order of magnitude faster than the steady state velocity. Similar transient response occurs in silicon and GaN. This transient "ballistic" transport can be used for pure ballistic transient devices operating at frequencies above several THz. However, these devices need to operate at very low voltages and produce limited power. The overshoot degrades more conventional TUNNETT operation. A brief summary of this operation is given in the next section.

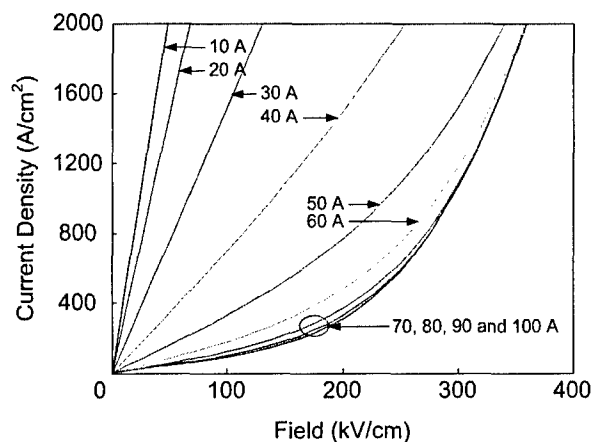


Fig. 29 - Tunneling properties for different barrier widths.

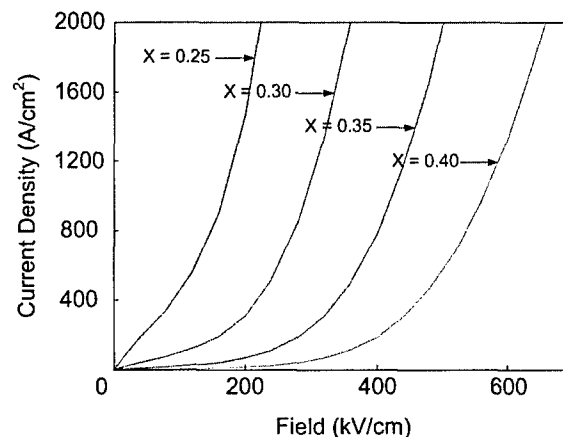


Fig. 30 - Transport properties for different barrier Al fractions.

**THz TUNNET Device Operation** - The injection calculations and transit transport results were combined to study the THz performance of TUNNETT devices. Typical waveforms for a device at 320 GHz are shown in Fig. 32. The red curve is the voltage across the structure, the green curve is the induced current based on the Monte Carlo transient simulation and the blue curve is the induced current based on an equilibrium transport approximation. The goal in a transit time device design is to reduce the induced current in the first half of the RF period and to increase it in the second half. The combination of the overshoot and the tunneling injection is having the opposite effect. Even though the transient overshoot time is a small fraction of an RF period it's effect is spread out over most of the first half of the RF cycle by the tunneling barrier. The larger current between  $\pi/2$  and  $\pi$  phase degrades the power available from the device. Similar effects occur for other material systems.

**Ballistic Operation** - As was reported in [16] and through subsequent calculations, we have shown that the frequency characteristics of the THz-range ballistic transit-time oscillator with a tunnel electron emission (ballistic TUNNETT-oscillator) suggested in the same works [16,17] does not only depend substantially on parameters of the transit space (drift region) but also specifically on the AC component of the tunnel emission current. If frequencies are low, this AC component is defined by the differential transparency of the tunnel emitter, and does not depend on the frequency. But it is known [18,19] that such a quasistatic approach may be unsuitable in the THz range because the so-called time of tunneling becomes comparable to the AC period or even exceeds it. Inadequacy of the quasistatic approach can be confirmed by our recent article [20] where we have developed an analytic theory of the ballistic TUNNETT, which can be constructed in the asymptotic case of the saturated nonparabolic dispersion relation for electrons:  $\varepsilon(p) = V_S(p-p_S)$  where  $V_S$  is a saturated ballistic velocity. In this case, we can display a certain connection between the optimal values of  $\sigma_S(\omega)$  (that optimize the quality factor of the device) and the frequency  $\omega$ :  $\sigma_S(\omega) \approx \omega \kappa_D(\omega)$  where  $\kappa_D(\omega)$  is a dielectric constant. To provide such a connection in the quasistatic case, we have to thin our tunnel barrier with an increase in  $\omega$ . This thinning leads to an increase in the direct current component and to a decrease in the device efficiency. The situation can be changed in the case when the quasistatic approach fails and the sufficiently large values of  $\sigma_S(\omega)$  can be reached by using the AC tunneling with the virtual absorption of the AC photon having the energy  $\hbar\omega$ . Such an effect [21] takes place in the intermediate region of the frequencies and the amplitudes of the AC electric field. The tunnel barrier is too thick for the direct tunneling of the electron with the Fermi energy  $\varepsilon_F$  but is much more transparent for electrons with the energy  $\varepsilon_F + \hbar\omega$ . With a subsequent increase in the AC field intensity, an increase in the DC tunnel current with the real (not virtual)  $\hbar\omega$  photon absorption leaves behind the above-mentioned virtual process and the efficiency falls again.

**Future Work** - The results in this report show the limitations on the power available from TUNNETT devices due to the physics of tunneling and transient transport. However these simulation tools can be used to overcome these limitations and improve the operation. The tunneling injection limitation can be overcome by designing for a small amount of avalanche generation in the structure. This will increase the current density, narrow the injected pulse and delay the peak phase. All of these effects will improve the performance. The avalanche will have little effect on the transient carrier overshoot. However proper design of the injector should move the peak of the induced current shown in Fig. 32 from before to after the  $\pi$  phase point. The same physical effect that was degrading the performance in the pure tunneling mode will be improving it for the mixed mode design. It can be seen from the simulation results that phonon scattering actually aids the performance in such devices and will help in identifying proper material systems.

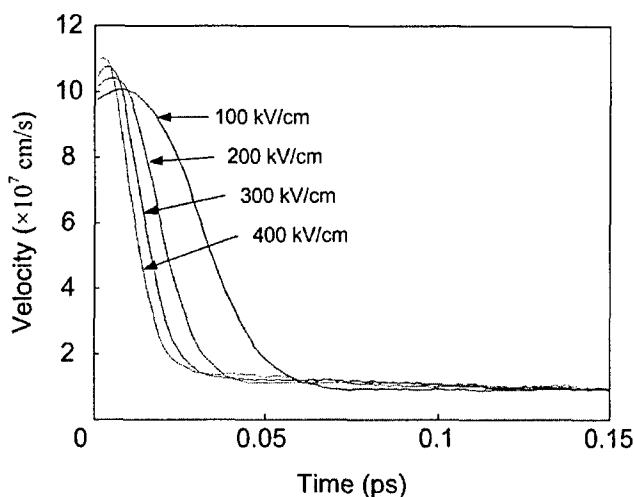


Fig. 31 - Transit response for electrons in GaAs.

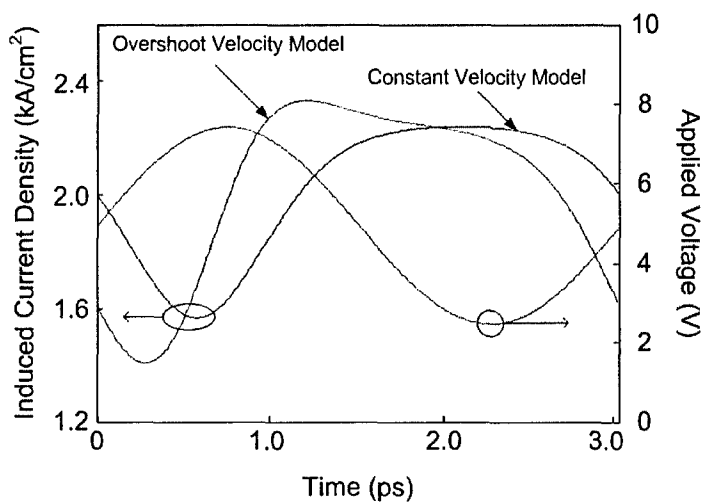


Fig. 32 - RF voltage and induced current waveforms for 320 GHz GaAs TUNNETT.

## 2.2.7 PHONON ENGINEERING IN Si AND GaAs HETEROSTRUCTURES: LIGHT EMITTERS

During this program, research at Wang's group focused on Si light emitting diodes. The schematic configuration of their Si LEDs is shown in Fig. 33. Three photolithography processes were used to fabricate the Si LEDs. Their processing began with a wet oxidation on an *n*-type Si wafer at 1000 °C for 30 min to grow 5000 Å wet oxide. After patterning the active areas of  $0.15 \times 0.15 \text{ cm}^2$  for electroluminescence measurements, a boron implant at an energy of 30 keV and a dose of  $1.0 \times 10^{15} \text{ cm}^{-2}$  was carried out, followed by an anneal at 600 and 1100 °C for 60 s in an RTP 610 rapid thermal processor in an  $\text{N}_2$  ambient. We used aluminum in direct contact with the implanted active areas as the *p*-side

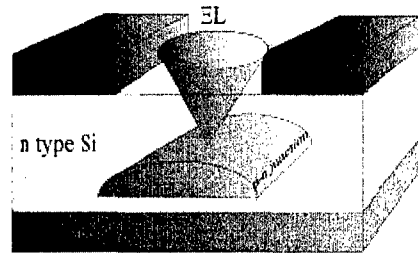


Fig. 33 - Schematics of the silicon LED.

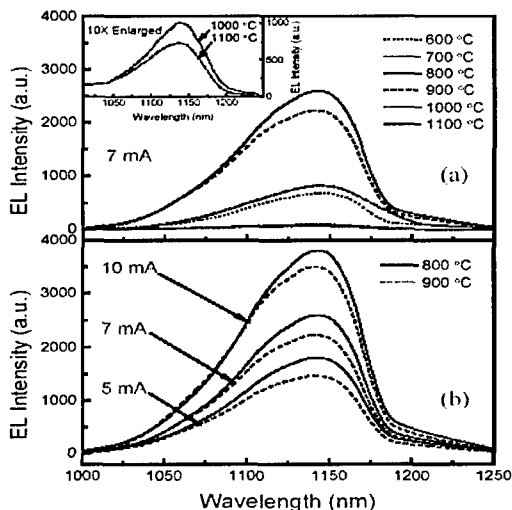


Fig. 34 - EL data of Si LEDs (a) EL data at constant current (7 mA) (b) EL characteristics of the LEDs annealed at 800 and 900 °C at currents of 5, 7 and 10 mA.

contact. The Al was sputtered in a

CVC 601 sputtering system at room temperature with a vacuum of  $2 \times 10^{-6}$  Torr prior to deposition. The backside electrode was made of Au, which was lift emission of the LEDs annealed at 600 and 700 °C is intermediate between those annealed at 800 and 900 °C, and those at 1000 and 1100 °C. Fig. 34 compares the EL characteristics of the LEDs annealed at 800 and 900 °C at currents of 5, 7 and 10 mA. For the three currents, we see that the emission of LEDs annealed at 800 °C is always higher than that of LEDs annealed at 900 °C. In summary, we fabricated, characterized and investigated Si LEDs. We found optimum processing conditions leading to the significant emission intensity enhancement. It is expected that their work on fabrication and characterization of Si LEDs will be continued so that, by the end of 2006, they plan to achieve a further increase in the EL intensity by the optimization of Si LED structure and fabrication process. Research will be addressed to the doping profiles optimization, growth condition improvement, and after growth temperature treatment. They also plan to demonstrate phonon-assisted luminescence enhancement in Si/Ge/Si tunnel diodes and in the modified Si Esaki diodes as well.

## 2.2.8 DILUTE NITRIDE GROWTH FOR PHONON ENGINEERING

During the considered period, Goldman's group pursued investigations of the epitaxial growth of GaAsN and InGaAsN using their Reactive Molecular Beam Epitaxy (RMBE) system, towards the development of advanced heterostructures for phonon-dispersion engineering. Goldman's group made significant progress in optimizing the growth of these alloy films which for the development of InGaAsN-based heterostructures for phonon dispersion engineering. In particular, correlations were examined between the growth, structure, electronic, and optical properties of InGaAsN films and heterostructures grown by solid-source molecular beam epitaxy using an  $\text{N}_2$ -RF plasma source.

**Epitaxial Growth: Nitrogen Plasma Chamber** - With partial support of this MURI program, Goldman's group upgraded their MBE system to include a separately valved and pumped chamber for the rf plasma source. The availability of this plasma chamber enables them to grow heterostructures with controlled nitrogen incorporation in successive layers, a capability not available in most MBE systems equipped for growth of GaInNAs and related materials. Figures 34(a) and (b) show the old and new configurations of the rf plasma source. In the old configuration, shown in Fig. 34(a), which is typical of most MBE systems, the nitrogen flux is controlled by a standard shutter; in this case, nitrogen incorporation into GaAs films occurs even with the shutter closed. For example, for a flux which results in 3% N in GaAsN, 0.1% N is incorporated when the shutter is closed, as revealed by the x-ray rocking curves (not shown). In the new configuration, shown in Fig. 34(b), the RF plasma source is contained in an independently turbo-pumped chamber attached to the MBE source flange via a pneumatic gate valve. In this case, the

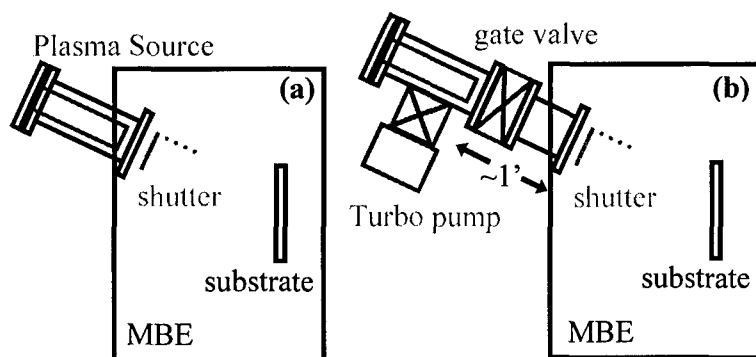


Fig. 34 - (a) original plasma source configuration, with nitrogen flux controlled by a shutter; (b) plasma source configuration with separately pumped and valved plasma chamber.

pneumatic gate valve is used to control the nitrogen flux, such that layers may be grown with and without nitrogen. This allows the researcher to grow well-controlled and high quality multilayers and heterostructures, resulting in record electron mobility values for modulation-doped heterostructures, as will be discussed below.

**Controlling the Nitrogen Composition-** For low N compositions in InGaAsN, many groups have found that the group V sticking coefficients are close to unity, suggesting that the N incorporation is inversely proportional to the group III growth rate [22]. For example, Fig. 35 presents a plot of N composition vs. the inverse GaAs growth rate, for a variety of plasma source configurations and source gases. The different symbols in the plot are distinguished by the N partial pressure (determined by the RGA described above). For both the original and modified plasma source configurations [Figs. 34(a) and 34(b)], the data fits a linear-least squares fit fairly well, consistent with the nearly unity group V sticking coefficients. In the case of the new source configuration with N<sub>2</sub>/Ar gas mixtures, shown as the blue triangles in Fig. 35, significantly lower nitrogen incorporation was observed for growth rates and nitrogen partial pressures similar to those used with the original plasma source configuration. In the modified source configuration, the plasma cell was shifted away from the substrate position by nearly 30 cm, as shown in Fig. 31(b), perhaps reducing the flux of active nitrogen radicals impinging on the sample. When pure N<sub>2</sub> is instead used as the source gas, N incorporation up to 5% is observed, as shown by the red circles in Fig. 35.

**In-Situ Characterization: Forbidden Window of Growth** - Using a reflection high energy diffraction (RHEED) system, in conjunction with ex-situ measurements, Goldman's group has recently identified a "forbidden window" for MBE growth of GaAsN, in the temperature range between ~ 460°C and 510°C. Growth outside the "forbidden window" is likely to lead to optimum properties. The reconstructions both inside and outside the "forbidden window" are mapped onto the GaAs surface phase diagram in Fig. 36. It is interesting to note that the "forbidden window" tends to occur in the vicinity of phase-boundaries in the GaAs surface phase diagram. Fig. 37 (a)-(h) shows RHEED patterns during the growth of GaAs<sub>1-x</sub>N<sub>x</sub> layers, collected along the [110] and [1 $\bar{1}$ 0] axes. During the growth of the 580°C GaAs buffer layer, RHEED revealed a streaky (2×4) pattern (not shown). For growth of GaAs<sub>1-x</sub>N<sub>x</sub> layers in the range 400-425°C, a streaky (2×1) RHEED pattern is apparent, as shown in Figs. 36 (a) and (b)[23,24]. As the growth temperature is increased from 460°C, a spotty (1×1) pattern appears, as shown in Figs. 36 (c) and (d). For higher temperatures, in the range 520-550°C, the pattern becomes a slightly spotty (3×1) pattern, which later converts to a streaky (3×4) pattern at 580°C, as shown in Figs. 36 (e) and (f), and (g) and (h), respectively. The (3×4) pattern is in contrast to the (3×3) pattern reported in some earlier work [24,25].

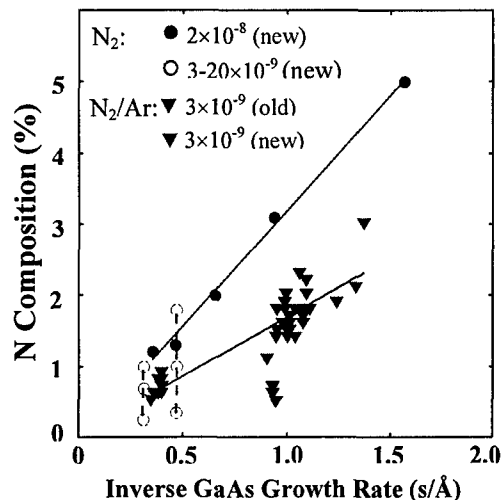


Fig. 35 - N composition vs. inverse GaAs growth rate, for various plasma configurations and source gases

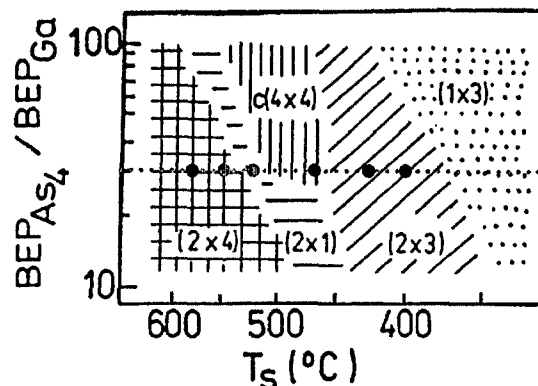
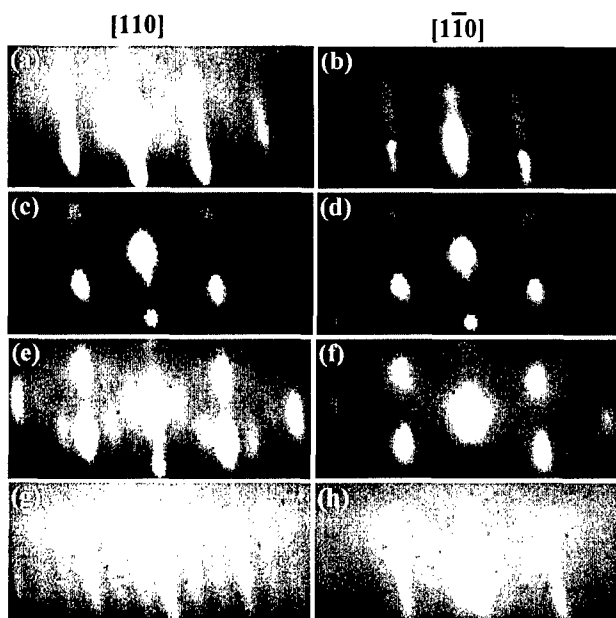


Fig. 36 (top) - Surface phase diagram for (001) GaAs. Colored dots indicate positions on diagram for GaAsN surface reconstructions in Fig. 37 [26].

Fig. 37 (left) - RHEED patterns collected along the [110] and [1-10] axes during growth of GaAsN films at (a) and (b) 400 - 425°C, (c) and (d) 460°C, (e) and (f) 520 - 550°C, and (g) and (h) 580°C.

**Multi-Beam Optical Stress Sensor Measurements** - Goldman's group has also used multi-beam optical stress sensor (MOSS) measurements to monitor the relaxation of stress during the growth of GaAsN films. These measurements allow them to determine both stress relaxation mechanisms and fundamental elastic properties, both of which are needed for optimum design of heterostructures for phonon dispersion engineering. In the MOSS measurement, shown in Fig. 38, a laser beam is passed through an etalon in order to produce three parallel output beams. These beams subsequently pass through the center viewport of the MBE source flange, and are reflected from the sample, back through the viewport, and into a CCD camera. Monitoring fractional changes in the spacing between these reflected spots,  $\delta d/d_0$ , or the mean differential spacing (MDS), enables a direct measurement of changes in the wafer radius of curvature. The radius of curvature is in turn related to the stress in the film,  $\sigma$ , using Stoney's Equation. Using the convention that decreasing beam spacing is negative, and tensile stress is positive, the stress  $\times$  thickness product,  $\sigma h_f$ , is related to the MDS as follows:

$$\sigma h_f = - \left( \frac{\delta d}{d_0} \right) \frac{M_s h_s^2 \cos \alpha}{12L}$$

where  $\alpha$  is the angle of incidence, measured with respect to the sample normal,  $L$  is the total optical path length from the sample surface to the detector,  $M_s$  is the biaxial modulus of the substrate, and  $h_s$  and  $h_f$  are the substrate and film thickness, respectively. Goldman's group has examined the effects of increasing N composition on the elastic constants of GaAsN alloys. A comparison of stresses determined using in-situ measurements of wafer curvature (MOSS) with those determined from x-ray rocking curves (XRC) using a linear interpolation of lattice and elastic constants is shown in Fig. 39 (a). In both cases, the composition was independently measured using nuclear reaction analysis. For N compositions  $> 1.3\%$ , the XRC stresses are higher than the MOSS stresses, presumably due to bowing of the elastic constants in  $\text{GaAs}_{1-x}\text{N}_x$ :

$$C_{ij}(\text{GaAs}_{1-x}\text{N}_x) = x C_{ij}(\text{GaN}) + (1-x) C_{ij}(\text{GaAs}) - b_{ij} x (1-x)$$

where a linear interpolation (i.e. Vegard's Law) assumes  $b_{ij}=0$ , and non-zero values of  $b_{ij}$  imply bowing of the elastic proper-

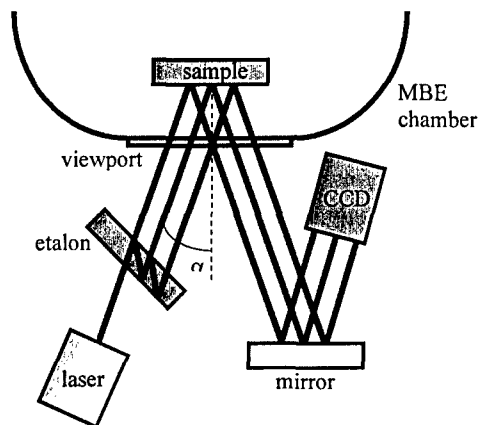


Fig. 38 - Schematic diagram of the multi-beam optical stress sensor. The laser beam is split into multiple beams by the etalon, which are reflected into a CCD camera that monitors the spacing of the beams.

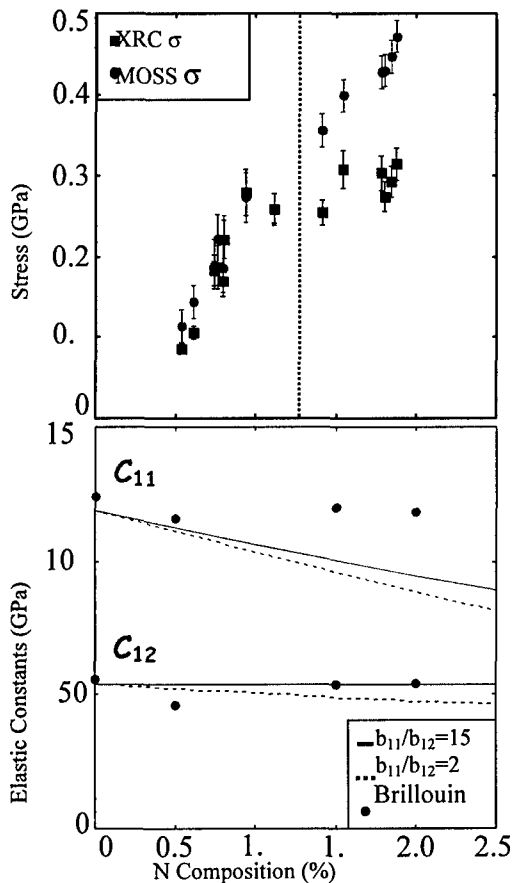


Fig. 39 - (a) Stress measured by in-situ MOSS and calculated from ex-situ XRC measurements, using a linear interpolation of lattice parameters and elastic constants; The stress differences in (a) are used to determine the composition dependence of the elastic constants, which are compared with Brillouin scattering measurements in (b).

regions between the elongated holes. In Fig. 40 (c), after 0.3 nm GaAsN growth, a nearly continuous film is observed. The GaAsN films also possess a  $4\times$  periodicity, with a lattice parameter slightly larger than that of GaAs. These results suggest that N atoms tend to occupy interstitial sites at the earliest stage of growth. In the future, Goldman's group plans to use the feedback from in-situ STM to identify the appropriate growth conditions which will allow the tuning of interstitial N incorporation, N cluster formation, and alloy phase separation, in both GaAsN and InGaAsN.

**Ex-Situ Characterization: Ion Beam Analysis-** To determine the substitutional and/or interstitial incorporation of N in InGaAsN alloys and heterostructures, Goldman's group used a combination of Rutherford Backscattering Spectrometry (RBS) and Nuclear Reaction Analysis (NRA), in channeling and non-channeling conditions. This set of measurements enabled them to estimate the fraction of incorporated N atoms sitting in split interstitial sites, as shown in Fig. 41. To date, Goldman's group has successfully used this approach to study N incorporation in dilute GaAsN. Prior to their work [27], conflicting results had been reported regarding the mechanism of N incorporation [22,28,29] As

ties. Figure 39 (b) shows the composition dependence of  $C_{11}$  and  $C_{12}$  using  $b_{ij}$  for which MOSS and XRC stresses are equal, with a range of  $b_1/b_2$  ratios. The composition dependence of the elastic constants is compared with values determined using bulk Brillouin scattering measurements, interpreted using the density and refractive index of GaAs. Further experimental and computational work is needed to fully understand the origins of the N-composition-dependent bowing of the elastic properties.

**In-Situ Scanning Tunneling Microscopy-** Although the RHEED and MOSS data provide average information on the surface structure, Goldman's group has also used additional tools in order to understand and control the film formation processes on the near atomistic scale. They use a series of *in-situ* scanning tunneling microscopy (STM) "snapshots" obtained after a series of growth/quenching sequences. An example of in-situ STM studies of sequential layers during the growth of GaAsN are shown in Figs. 40 (a)–(c). For the 500 nm GaAs buffer shown in Fig. 40 (a), a  $4\times$  periodicity and  $[1\bar{1}0]$  elongated holes are apparent. After 0.1 nm GaAsN growth, shown in Fig. 40 (b), isolated domains nucleate on flat

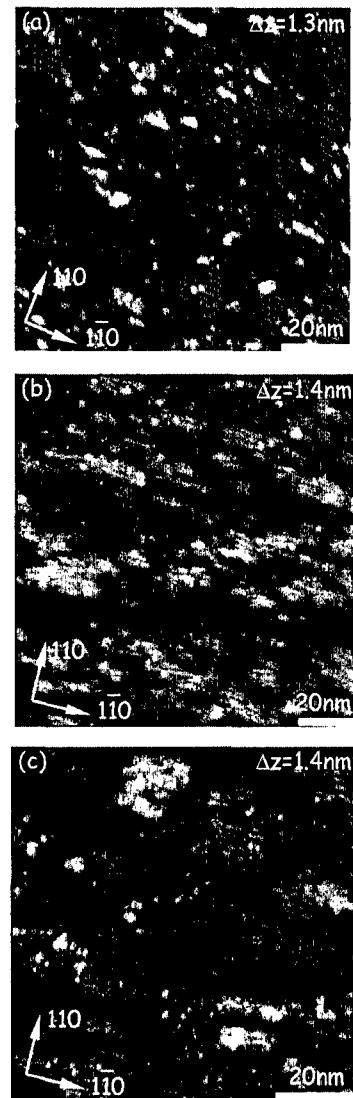


Fig. 40 - In-situ scanning tunneling microscopy images of sequential layers of (a) GaAs, (b) 0.1 nm GaAsN, and (c) 0.3 nm GaAsN. The gray-scale ranges displayed are (a) 1.3 nm, (b) 1.4 nm, and (c) 1.4 nm.

shown in Fig. 42, their studies revealed significant composition-dependent incorporation of N into non-substitutional sites, presumably as either N-N or N-As split interstitials. Furthermore, we identified the (2x1) reconstruction, associated with low growth temperatures, as the surface structure which leads to the highest substitutional N incorporation, likely due to the high number of group V sites per unit area available for N-As surface exchange.

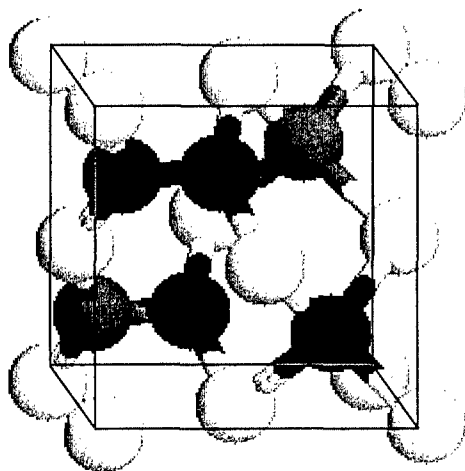


Fig. 41 - Ball and stick crystal schematic for GaAsN with substitutional N, N-As split interstitial, and N-N split interstitial. The white, green, and black spheres represent Ga, As, and N, respectively.

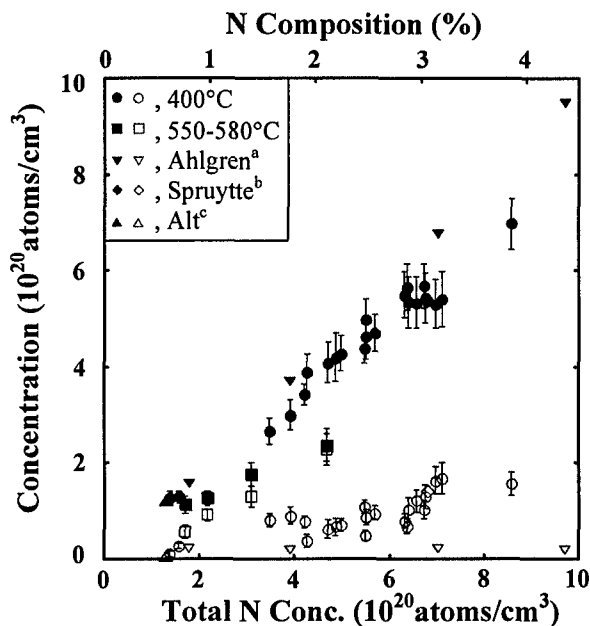


Fig. 42 - Substitutional (red) and interstitial (green) concentrations vs. total N concentration for GaAs<sub>1-x</sub>N<sub>x</sub> with varying x. The concentration of interstitial N increases with total N concentration. <sup>a</sup>See Ref. 28; <sup>b</sup>See Ref.22; <sup>c</sup>See Ref. 29.

**Electronic Transport Properties: Dilute Nitride Films** - To date, Goldman's group has systematically studied the effects of growth conditions on the electron mobility of GaAsN films, using the variations in nitrogen plasma source configurations discussed earlier. As shown in Figs. 43 (a) and 43 (b), the electron mobility of GaAsN films is strongly dependent on the plasma source gas and GaAs growth rate, respectively. In particular, the highest electron mobilities are apparent for films grown with pure N<sub>2</sub>, using higher growth rates. As shown in Fig. 43 (a), the electron mobilities of our GaAsN films grown in optimum conditions are most often higher than literature reports to date

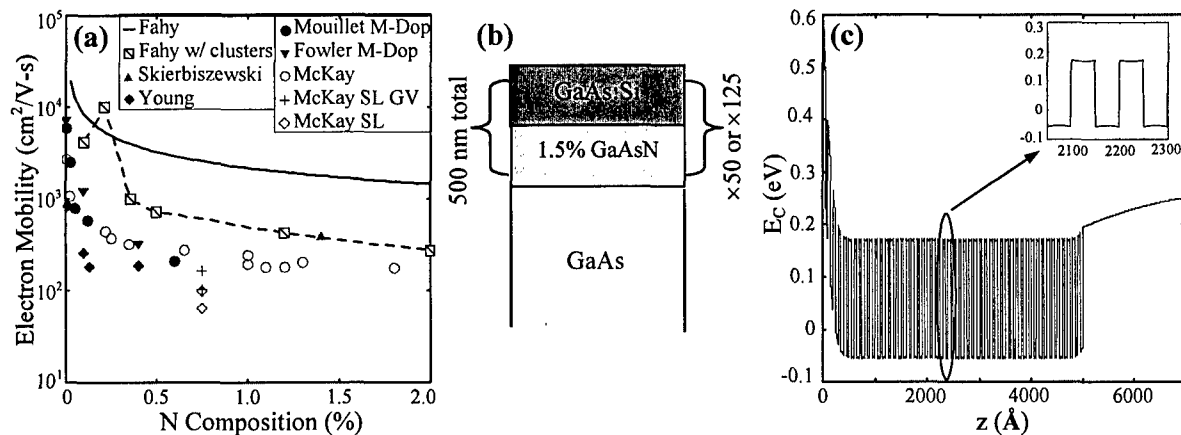


Fig. 43 - (a) Electron mobility vs. N composition for our GaAsN films (McKay), in comparison with other reports. The solid and dashed lines are calculated assuming all N substitutes for As, The dashed line includes the resonant scattering contribution from N clusters. In addition, the mobilities of GaAsN/GaAs:Si SLs, shown schematically in (b), are included in (a). The corresponding energy band diagram of the SLs in (b) is shown in (c).

Surface
100 Å, GaAs
600 Å, Al <sub>0.3</sub> Ga <sub>0.7</sub> As, Nd = 5*10 <sup>17</sup> cm <sup>-3</sup>
spacer layer 200 Å, Al <sub>0.3</sub> Ga <sub>0.7</sub> As
10 Å, GaAs
130 Å, GaAs <sub>0.999</sub> N <sub>0.001</sub>
10 Å, GaAs
500 Å, Al <sub>0.3</sub> Ga <sub>0.7</sub> As
3000 Å, GaAs
SI GaAs substrate

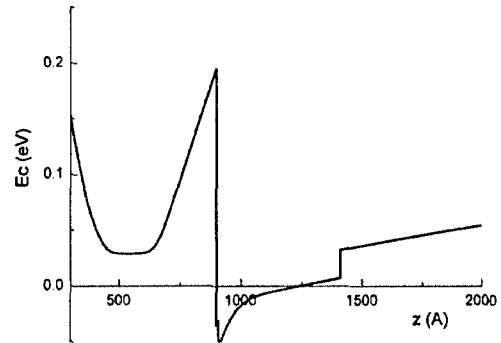


Fig. 44 - Cross-section of selectively doped GaAsN/AlGaAs heterostructure (left) and corresponding conduction energy band diagram (right). A two-dimensional electron gas is formed in the triangular quantum well potential in the GaAsN layer.

[30,31]. The most striking feature of this combined data is the steep drop electron mobility with N composition, a clear indication that N related defects are the main source of scattering in dilute nitrides. Yet, the highest measured electron mobilities are still about a factor two smaller than the recent calculations of electron scattering by Fahy *et al.* which include resonant scattering from N clusters [32].

**Superlattice Structures-** In principle, due to the modulation doping of Si in a doped/undoped superlattice (SL) structure, the electron mobility of a SL structure may be larger than a corresponding film with similar composition [33]. Figure 43 (b) presents a GaAsN/GaAs:Si heterostructure, with the corresponding conduction energy band diagram, calculated using the Poisson Solver. For this structure, the electron mobility was improved by the use of the gate-valve interface control in comparison with the conventional shuttering approach.

**GaAsN/AlGaAs heterostructures** - A selectively doped GaAsN/AlGaAs heterostructure and the calculated conduction band energy diagram of the corresponding structure are shown in Fig. 44. In such a structure a two-dimensional electron gas (2DEG) is formed in a triangular confinement potential in GaAsN. Similar to GaAs/AlGaAs heterostructures, the carrier density of the electron gas can be engineered by varying the spacer layer thickness. In collaboration with Kurdak's group, Goldman's group designed and grew a heterostructure with very low N composition (<0.05%). Remarkably, at low temperatures, in this very low N composition 2DEG structure, we observe integer quantum Hall effect and well-resolved Shubnikov de Haas oscillations at magnetic fields down to 1 Tesla, as shown in Fig. 45. The extracted the carrier density and the electron mobility of the 2DEG are  $1.13 \times 10^4 \text{ cm}^2/\text{Vs}$  and  $1.86 \times 10^{11} \text{ cm}^{-2}$ , respectively. The electron mobility of this 2DEG structure is substantially higher than those recently reported in the literature [22,31] presumably due to our gate-valve control of the heterostructure interfaces, described earlier.

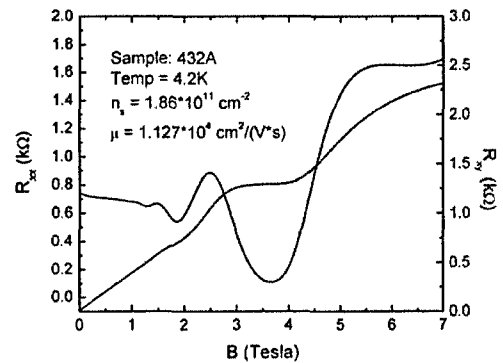


Fig. 45 - Quantum Hall effect and Shubnikov-de Haas data at 4.2 K from a GaAsN/AlGaAs heterostructure with a two-dimensional electron gas.

### 3. REFERENCES

- [1] D. H. Auston, K. P. Cheung, J. A. Valdmanis and D. A. Kleinman, "Cherenkov radiation from femtosecond optical pulses in electro-optic media," *Phys. Rev. Lett.* **53**, 001555 (1984)
- [2] T. E. Stevens, J. K. Wahlstrand, J. Kuhl and R. Merlin, "Cherenkov Radiation at Speeds Below the Light Threshold: Phonon Assisted Phase Matching," *Science* **291**, 627-630 (2001).
- [3] P. H. Bucksbaum and R. Merlin, "The Phonon Bragg Switch: A Proposal to Generate Sub-Picosecond X-Ray Pulses," *Solid State Commun.* **111**, 535-539 (1999).
- [4] M. F. DeCamp, D. A. Reis, P. H. Bucksbaum, B. Adams, J. M. Caraher, R. Clarke, C. W. S. Conover, E. M. Dufresne, R. Merlin, V. Stoica and J. K. Wahlstrand, "Coherent Control of Pulsed X-Ray Beams," *Nature* **413**, 825-829 (2001).
- [5] H. T. Grahn, H. J. Maris and J. Tauc, "Picosecond ultrasonic," *IEEE J. Quantum Electron.* **25**, 2562-2569 (1989).
- [6] T. E. Stevens, J. Kuhl and R. Merlin, "Coherent Phonon Generation and the Two Stimulated Raman Tensors," *Phys. Rev. B* **65**, 144304 (2002).
- [7] C. Aku-Leh, J. Zhao, R. Merlin, J. Menéndez and M. Cardona, "Long-lived optical phonons in ZnO studied with impulsive stimulated Raman scattering," *Phys. Rev. B* **71**, 205211 (2005).
- [8] I. H. Lee, K. J. Yee, K. G. Lee, E. Oh, D. S. Kim and Y. S. Lim, "Coherent optical phonon mode oscillations in wurtzite ZnO excited by femtosecond pulses," *J. Appl. Phys.* **93**, 4939 (2003).
- [9] A. V. Bragas, C. Aku-Leh and R. Merlin, "Raman and ultrafast optical spectroscopy of acoustic phonons in  $\text{Cd}_{0.68}\text{Te}_{0.32}\text{Se}$  quantum dots," *Phys. Rev. B* **73**, 125305 (2006).
- [10] U. Ozgur, C. W. Lee and H. O. Everitt, "Control of coherent acoustic phonons in semiconductor quantum wells," *Phys. Rev. Lett.* **86**, 5604 (2001).
- [11] U. Ozgur, H. O. Everitt, L. He and H. Morkoc, "Stimulated emission and ultrafast carrier relaxation in Al-GaN/GaN multiple quantum wells," *Appl. Phys. Lett.* **82**, 4080 (2003).
- [12] B. C. Daly, N. C. R. Holme, T. Buma, C. Branciard, T. B. Norris, D. M. Tennant, J. A. Taylor, J. E. Bower and S. Pau, "Imaging nanostructures with coherent phonon pulses," *Appl. Phys. Lett.* **84**, 5180 (2004).
- [13] H. Karl, W. Dietsche, A. Fischer and K. Ploog, "Imaging of the Phonon-Drag Effect in GaAs-AlGaAs Heterostructures," *Phys. Rev. Lett.* **61**, 2360 (1988).
- [14] B. C. Daly, T. B. Norris, J. Chen and J. B. Khurgin, "Picosecond acoustic phonon pulse propagation in silicon," *Phys. Rev. B* **70**, 214307 (2004).
- [15] J. Chen and J. B. Khurgin, "Optical phonons in a periodically inverted polar superlattice," *Phys. Rev. B* **70**, 085319 (2004).
- [16] Z. S. Gribnikov, N. Z. Vagidov, V. V. Mitin, and G. I. Haddad, "Ballistic and quasiballistic tunnel transit time oscillators for the terahertz range: linear admittance," *J. Appl. Phys.* **93**, pp. 5435-5446 (2003).
- [17] Z. S. Gribnikov, N. Z. Vagidov, V. V. Mitin, and G. I. Haddad, "Theory of unipolar ballistic and quasiballistic transit-time oscillators for a terahertz range," *Physica E* **19**, pp. 89-94 (2003)
- [18] M. Buttiker and R. Landauer, "Traversal time for tunneling," *Phys. Rev. Lett.* **49**, 1739-1742 (1982).
- [19] R. Landauer and Th. Martin, "Barrier interaction time in tunneling," *Rev. Mod. Phys.* **66**, 217-228 (1994).
- [20] Z. S. Gribnikov, N. Z. Vagidov, and G. I. Haddad, "Phenomenological theory of a tunnel emitter transit time oscillators for the terahertz range," *J. Appl. Phys.* **95**, pp. 1489-1496 (2004).
- [21] Z. Gribnikov and G. Haddad, "Theory of heterostructural tunnel emitters for ballistic transit-time terahertz-range oscillators (abstract)," *27th Int. Conf. Phys. Semicond (ICPS-27)*, July 26-30, 2004, Flagstaff, Arizona, USA, **Q5 96**, p.318.
- [22] S. G. Spruytte, C. W. Coldren, J. S. Harris, W. Wampler, P. Krispin, K. Ploog, and M. C. Larson, "Incorporation of nitrogen in nitride-arsenides: Origin of improved luminescence efficiency after anneal," *J. Appl. Phys.* **89**, 4401 (2001).

- 
- [23] M. Reason, W. Ye, X. Weng, G. Obeidi, V. Rotberg, and R. S. Goldman, "Stress Evolution in GaAsN Films Grown by Reactive Molecular Beam Epitaxy", Proc. Nat. Center for Photovoltaics and Solar Program Review, (2003).
- [24] M. A. Pinault and E. Tournie, "Influence of alloy stability on the photoluminescence properties of GaAsN/GaAs quantum wells grown by molecular beam epitaxy", Appl. Phys. Lett. **79**, 3404 (2001).
- [25] A. R. Kovsch, J. S. Wang, L. Wei, R. S. Shaio, J. Y. Chi, B. V. Volovik, A. F. Tsatsulnikov, and V. M. Ustinov, "Effects of surface nitridation during nitrogen plasma ignition on optical quality of GaInAsN grown by solid source molecular beam epitaxy", J. Vac. Sci. Technol. B **20**, 1158 (2002).
- [26] L. Daweritz and R. Hey, "Reconstruction and defect structure of vicinalGaAs(001) and Al<sub>x</sub>Ga<sub>1-x</sub>As(001) surfaces during MBE growth", Surf. Sci. **236**, 15 (1990).
- [27] M. Reason, H. A. McKay, W. Ye, S. Hanson, V. Rotberg, and R. S. Goldman, "Mechanisms of nitrogen incorporation in GaAsN alloys", Appl. Phys. Lett. **85**, 1692 (2004).
- [28] T. Ahlgren, Vainonen-Ahlgren, J. Likonen, W. Li, and M. Pessa, "Concentration of interstitial and substitutional nitrogen in GaNAs", Appl. Phys. Lett. **80**, 2314 (2002).
- [29] H. C. Alt, A. Y. Egorov, H. Riechert, J. D. Meyer, and B. Wiedemann, "Incorporation of nitrogen in GaAsN and InGaAsN alloys investigated by FTIR and NRA", Physica B **308-310**, 877 (2001).
- [30] C. Skierbiszewski, P. Perlin, P. Wisniewski, T. Suski, W. Walukiewicz, W. Shan, J. W. Ager, E. E. Haller, J. F. Geisz, D. J. Freidman, J. M. Olson, and S. R. Kurtz, "Effect of Nitrogen-Induced Modification of the Conduction Band Structure on Electron Transport in GaAsN Alloys", Phys. Stat. Sol. B **216**, 135 (1999).
- [31] D. Fowler, O. Makarovsky, A. Patane, L. Eaves, L. Geelhaar, and H. Reichert, "Electron conduction in two-dimensional GaAsN channels", Phys. Rev. B **69**, 153305 (2004).
- [32] S. Fahy, A. Lindsay, and E. P. O'Reilly, "Intrinsic limits on electron mobility in disordered dilute nitride semiconductor alloys", IEE Proc. Opto. **151**, 352 (2004).
- [33] Y. G. Hong, C. W. Tu, and R. K. Ahrenkiel, "Improving properties of GaInNAs with a short-period GaInAs/GaNAs superlattice", J. Cryst. Growth **227-228**, 536 (2001).

#### 4. PERSONNEL SUPPORTED

PI's	Graduate Students		Postdoctoral Associates	Research Scientists
P. K. Bhattacharya	Cynthia Akuleh (UM)	Jianlin Liu (UCLA)	Andrea Bragas (UM)	Heribert Eisele (UM)
R. Goldman	Xiaogang Bai (UM)	Roman Ostroumov (UCLA)	Toby Eckhause (UM)	A. Khitun (UCLA)
G. Haddad	R. Bashirov (UM)	Matt Reason (UM)	Sergiy Komirenko (NCSU)	Z. Gribnikov (UM)
J. B. Khurgin	J. Chen (JH)	Özgün Süzer (UM)	Ümit Özgür (VCU)	Brian Daly (UM)
K. W. Kim	Baron Phillip (UCLA)	Jared Wahlstrand (UM)		
C. Kurdak	Carl Fischer (UM)	Xiaojun Weng (UM)		
R. Merlin	Siddhartha Ghosh (UM)	Weifeng Ye (UM)		
H. Morkoç	Jaeil Kim (UM)	Jimin Zhao (UM)		
M. Msall	Kyoung Kim (UM)			
T. Norris				
K. Wang				

The MURI grant also supported visits of Prof. V. Mitin and Dr. N. Vagidov (Wayne State University, MI) to the University of Michigan for interactive research, and Prof. V. A. Kochelap and Dr. B. Glavin to NCSU.

#### 5. PUBLICATIONS SUPPORTED BY F49620-00-1-0328

1. "Coherent optical phonon generation by the electric current in quantum wells." S. M. Komirenko, K. W. Kim, V. A. Kochelap, I. Fedorov, and M. A. Stroscio, *Appl. Phys. Lett.* **77**, 4178 (2000).
2. "Generation and amplification of sub-THz coherent acoustic phonons under the drift of 2D-electrons." S. M. Komirenko, K. W. Kim, A. A. Demidenko, V. A. Kochelap, and M. A. Stroscio, *Phys. Rev. B* **62**, 7459 (2000).
3. "Modification of the three-phonon Umklapp process in a quantum wire." A. Khitun and K. L. Wang, to be published in *Appl. Phys. Lett.* **79**, 851 (2001).
4. "Systematic measurements of  $\text{Al}_x\text{Ga}_{1-x}\text{N}$  refractive indices." U. Ozgur, G. Webb-Wood, H. O. Everitt, F. Yun and H. Morkoç, *Appl. Phys. Lett.* **79**, 4103 (2001).
5. "Amplification of transverse acoustic phonons in QW heterostructures with piezoelectric interaction." S. M. Komirenko, K. W. Kim, A. A. Demidenko, V. A. Kochelap, and M. A. Stroscio, *J. Appl. Phys.* **90**, 3934 (2001).
6. "Coherent Control of Pulsed X-Ray Beams." M. F. DeCamp, D. A. Reis, P. H. Bucksbaum, B. Adams, J. M. Caraher, R. Clarke, C. W. Conover, E. Dufresne, R. Merlin, V. Stoica and J. Wahlstrand, *Nature* **413**, 825-829 (2001).
7. "Generation of coherent confined optical phonons under the drift of two-dimensional electrons." S. M. Komirenko, K. W. Kim, V. A. Kochelap, I. Fedorov, and M. A. Stroscio, *Phys. Rev. B* **63**, 165308 (2001).
8. "Dynamics and Coherent Control of High Amplitude Optical Phonons in Bismuth." M. F. DeCamp, D. A. Reis, P. H. Bucksbaum and R. Merlin, *Phys. Rev. B* **64**, 092301 (2001).
9. "Probing Impulsive Strain Propagation with X-Ray Pulses." D. A. Reis, M. F. DeCamp, P. H. Bucksbaum, R. Clarke, M. Hertlein, R. Merlin, E. Dufresne, R. Falcone, H. C. Kapteyn, M. M. Murnane, J. Larsson, Th. Misaalla and J. Wark, *Phys. Rev. Lett.* **86**, 3072 (2001).

10. "Observation of Phonon Bottleneck in Quantum Dot Electronic Relaxation." J. Urayama, T. B. Norris, J. Singh and P. Bhattacharya, *Phys. Rev. Lett.* **86**, 4930 (2001).
11. "Cherenkov Radiation at Speeds Below the Light Threshold: Phonon Assisted Phase Matching." T. E. Stevens, J. K. Wahlstrand, J. Kuhl and R. Merlin, *Science* **291**, 627 (2001).
12. "Hall Mobility and Carrier Concentration in Free-Standing High Quality GaN Templates Grown by Hydride Vapor Phase Epitaxy." D. Huang, F. Yun, M. A. Reshchikov, D. Wang, H. Morkoç, D. L. Rode, L. A. Farina, Ç. Kurdak, K. T. Tsen, S. S. Park, and K. Y. Lee, *Solid State Electron.* **45**, 711 (2001).
13. "The effect of the long-range order in a quantum dot array on the in-plane lattice thermal conductivity." A. Khitun, A. Balandin, J. L. Liu and K. L. Wang, *Superlattices and Microstructures* **30**, 1 (2001).
14. "Temperature Dependence of Carrier Dynamics in Self-Organized Quantum Dots." J. Urayama, T. B. Norris, J. Singh, and P. K. Bhattacharya, *Appl. Phys. Lett.* **80**, 2162 (2002).
15. "Stimulated Emission Induced Enhancement of the Decay Rate of Longitudinal Optical Phonons in III-V Semiconductors." J. Chen, J. Khurgin, R. Merlin, *Appl. Phys. Lett.* **80**, 2901 (2002).
16. "Tunnel injection In<sub>0.4</sub>Ga<sub>0.6</sub>As/GaAs quantum dot lasers with 15 GHz modulation bandwidth at room temperature." P. Bhattacharya and S. Ghosh, *Appl. Phys. Lett.* **80**, 3483 (2002).
17. "Gain Dynamics and Ultrafast Spectral Hole-Burning in In(Ga)As Self-Organized Quantum Dots." K. Kim, J. Urayama, T. B. Norris, J. Singh, J. Phillips, and P. K. Bhattacharya, *Appl. Phys. Lett.* **81**, 671 (2002).
18. "Acoustic Cavity Polariton in Multilayer Piezoelectric Structures." J. Chen, J. B. Khurgin, *Appl. Phys. Lett.* **81**, 4742 (2002).
19. "Temperature-dependent steady-state characteristics of high-performance tunnel injection quantum dot lasers." S. Pradhan, S. Ghosh, and P. Bhattacharya, *Electron. Lett.* **38**, 1449 (2002).
20. "Differential Transmission Measurement of Phonon Bottleneck in Self-Assembled Quantum Dot Intersubband Relaxation." J. Urayama, T. B. Norris, H. Jiang, J. Singh, and P. K. Bhattacharya, *Physica B* **316-317**, 74 (2002).
21. "Confinement and Amplification of Terahertz Acoustic Phonons in Cubic Heterostructures." S. M. Komirenko, K. W. Kim, V. A. Kochelap, and M. A. Stroschio, *Physica B* **316-317**, 356 (2002).
22. "Quantum Well Based Phonon Detectors: Performance Analysis." X. Bai, Ç. Kurdak, S. Krishna, and P. Bhattacharya, *Physica B* **316-317**, 362 (2002).
23. "Electron dispersion relation with negative effective mass in quantum wells grown on the cleaved edge of a superlattice." Z. Gribnikov, R. Bashirov, H. Eisele, V. Mitin, and G. Haddad, *Physica E* **12**, 276 (2002).
24. "Voltage-Controlled Generation of High-Frequency Coherent Acoustic Phonons in Superlattices." B. A. Glavin, V. A. Kochelap, T. L. Linnik, K. W. Kim, and M. A. Stroschio, *Physica E* **12**, 458 (2002).
25. "Generation of High-Frequency Coherent Acoustic Phonons in a Superlattice under the Hopping Transport: I. Linear Theory of Phonon Instability." B. A. Glavin, V. A. Kochelap, T. L. Linnik, K. W. Kim, and M. A. Stroschio, *Phys. Rev. B* **65**, 085303 (2002).
26. "Generation of High-Frequency Coherent Acoustic Phonons in a Superlattice under the Hopping Transport: II. Steady-State Phonon Population and Electric Current in the Generation Regime." B. A. Glavin, V. A. Kochelap, T. L. Linnik, K. W. Kim, and M. A. Stroschio, *Phys. Rev. B* **65**, 085304 (2002).
27. "Coherent Phonon Generation and the Two Stimulated Raman tensors." T. E. Stevens, J. Kuhl and R. Merlin, *Phys. Rev. B* **65**, 144304 (2002).
28. "Confinement and Amplification of Acoustic Waves in Cubic Heterostructures." S. M. Komirenko, K. W. Kim, V. A. Kochelap, and M. A. Stroschio, *Phys. Rev. B* **65**, 155321 (2002).
29. "Ballistic Phonon Production in Photoexcited Ge, GaAs, and Si." M. E. Msall and J. P. Wolfe, *Phys. Rev. B* **65**, 195205 (2002).
30. "Evolution of Microstructure and Optical Properties of GaAsN Nanostructures Synthesized by Ion Implantation." X. Weng, S. J. Clarke, W. Ye, S. Kumar, R. S. Goldman, V. Rotberg, J. Holt, J. Sipowska, A. Francis, A. Daniel, and R. Clarke, *J. Appl. Phys.* **92**, 4012 (2002).
31. "Optical phonons in self-assembled Ge quantum dot superlattices: strain relaxation effects." J. L. Liu, J. Wan, Z. M. Jiang, A. Khitun, and K. L. Wang, *J. Appl. Phys.* **92**, 6804 (2002).
32. "Stimulated Emission and Ultrafast Carrier Relaxation in InGaN Multiple Quantum Wells." Ü. Özgür, H. O. Everitt, S. Keller, and S. P. DenBaars, *Appl. Phys. Lett.* **82**, 1416 (2003).

33. "Observation of Optical Phonon Instability Induced by Drifting Electrons in Semiconductor Nanostructures." W. Liang, K. T. Tsen, O. F. Sankey, S. M. Komirenko, K. W. Kim, V. A. Kochelap, M.-C. Wu, C.-L. Ho, W.-J. Ho, and H. Morkoc, *Appl. Phys. Lett.* **82**, 1968 (2003).
34. "Electric Field Induced Heating and Energy Relaxation in GaN." T. A. Eckhause, Ö. Süzer, Ç. Kurdak, F. Yun and H. Morkoç, *Appl. Phys. Lett.* **82**, 3035 (2003).
35. "Stimulated Emission and Ultrafast Carrier Relaxation in AlGaIn/GaN Multiple Quantum Wells." Ü. Özgür, H. O. Everitt, L. He and H. Morkoç, *Appl. Phys. Lett.* **82**, 4080 (2003).
36. "Gouy Phase Shift of Single-Cycle Picosecond Acoustic Pulses." N. C. R. Holme, M. T. Myaing, and T. B. Norris, *Appl. Phys. Lett.* **83**, 392 (2003).
37. "Feasibility of Phonon Lasers." J. B. Khurgin, and J. Chen, *IEEE J. Quantum Electron.* **39**, 600 (2003),
38. "Nanoscale Thermal Transport." D. G. Cahill, W. K. Ford, K. E. Goodson, G. D. Mahan, H. J. Maris, A. Majumdar, R. Merlin and S. R. Phillpot, *J. Appl. Phys. (Appl. Phys. Reviews)* **93**, 793 (2003).
39. "Ballistic and quasiballistic tunnel transit time oscillators for the terahertz range: A linear admittance." Z. S. Gribnikov, N. Z. Vagidov, V.V. Mitin, and G. I. Haddad, *J. Appl. Phys.* **93**, 5435 (2003).
40. "Quantum real-space transfer in a heterostructure overgrown on the cleaved edge of a superlattice." Z. S. Gribnikov, N. Z. Vagidov, R. R. Bashirov, V.V. Mitin, and G. I. Haddad, *J. Appl. Phys.* **94**, 330 (2003).
41. "Negative effective mass terahertz range oscillators on a cleaved edge of a superlattice." Z. S. Gribnikov, N. Z. Vagidov, and V.V. Mitin, *J. Computat. Electron.* **2**, 5 (2003).
42. "Theory of unipolar ballistic and quasiballistic transit-time oscillators for the terahertz range." Z. S. Gribnikov, N. Z. Vagidov, V.V. Mitin, and G. I. Haddad, *Physica E* **19**, 89-94 (2003).
43. "Cross-plane thermal conductivity of self-assembled Ge quantum dot superlattices." J. L. Liu, A. Khitun, K. L. Wang, W. L. Liu, G. Chen, Q. H. Xie and S. G. Thomas., *Physical Review B* **67**, 165333 (2003).
44. "Cherenkov Radiation Emitted by Ultrafast Laser Pulses and the Generation of Coherent Polaritons." J. K. Wahlstrand and R. Merlin, *Phys. Rev. B* **68**, 054301 (2003).
45. "Nonlinear Regimes of Coherent Optical Phonon Generation under Electric Current Pumping." S. M. Komirenko, K. W. Kim, V. A. Kochelap, V. V. Koroteev and M. A. Strosio, *Phys. Rev. B.* **68**, 155308 (2003).
46. "Transient Strain Driven by a Dense Electron-Hole Plasma." M. F. DeCamp, D. A. Reis, A. Cavaliere, P. H. Bucksbaum, R. Clarke, R. Merlin, E. M. Dufresne, D. A. Arms, A. Lindenberg, A. MacPhee, Z. Chang, B. Lings, J. S. Wark, and S. Fahy, *Phys. Rev. Lett.* **91**, 165502 (2003).
47. "Mechanisms of Lateral Ordering of InAs/GaAs Quantum Dot Superlattices." W. Chen, B. Shin, R.S. Goldman, A. Stiff, and P.K. Bhattacharya, *J. Vac. Sci. Technol. B* **21**, 1920 (2003).
48. "Laser in Physics: Squeezed Phonons in Solids." A. V. Bragas and R. Merlin, to be published in *Encyclopedia of Modern Optics*, ed. by B. Guenther, A. Miller, L. Bayvel and J. Midwinter (Academic Press, London, 2003).
49. "Phenomenological theory of tunnel emitter transit time oscillators for terahertz range." Z. S. Gribnikov, N. Z. Vagidov and G. I. Haddad, submitted to *J. Appl. Phys* (2003).
50. "Analytical Solution of the Almost-Perfect-Lens Problem." R. Merlin, *Appl. Phys. Lett.* **84**, 1290-1292 (2004).
51. "Imaging nanostructures with coherent phonon pulses." B. C. Daly, N. C. R. Holme, T. Buma, C. Branciard, T. B. Norris, D. M. Tennant, J. A. Taylor, J. E. Bower and S. Pau, *Appl. Phys. Lett.* **84**, 5180 (2004).
52. "On the modeling of lattice thermal conductivity in semiconductor quantum dot superlattice." A. Khitun, J. L. Liu and K. L. Wang, *Appl. Phys. Lett.* **84**, 1762 (2004).
53. "Mn-doped InAs self-organized diluted magnetic quantum-dot layers with Curie temperatures above 300 K." M. Holub, S. Chakrabarti, S. Fathpour, P. Bhattacharya, Y. Lei and S. Ghosh, *Appl. Phys. Lett.* **85**, 973 (2004).
54. "Mechanisms of Nitrogen Incorporation in GaAsN Alloys." M. Reason, H. McKay, W. Ye, S. Hanson, V. Rotberg, and R.S. Goldman, *Appl. Phys. Lett.* **85**, 1692 (2004).
55. "Origins of Luminescence from Nitrogen Ion Implanted Epi-GaAs." X. Weng, R. S. Goldman, V. Rotberg, N. Bataiev, and L.J. Brillson, *Appl. Phys. Lett.* **85**, 2774 (2004).
56. "Photoelectric response of polarization sensitive bacteriorhodopsin films." Q. Li, J. A. Sturat, R. R. Birge, et al. *Biosensors & Bioelectronics* **19**, 869 (2004).
57. "Monolithically integrated bacteriorhodopsin/semiconductor opto-electronic integrated circuit for a biophotoreceiver." J. Xu, P. Bhattacharya, G. Vargo, *Biosensors & Bioelectronics* **19**, 885 (2004).
58. "Phenomenological theory of a tunnel emitter transit time oscillators for the terahertz range." Z. S. Gribnikov, N. Z. Vagidov and G. I. Haddad, *J. Appl. Phys.* **95**, 1489 (2004).

59. "Tunable normal incidence Ge quantum dot midinfrared detectors." S. Tong, F. Liu, A. Khitun, et al. *J. Appl. Phys.* **96**, 773 (2004).
60. "Time-dependent electron tunneling through time-dependent tunnel barriers." Z. S. Gribnikov and G. I. Haddad, *J. Appl. Phys.* **96**, 3831 (2004).
61. "Photoluminescence and deep levels in lattice-matched InGaAsN/GaAs," C. H. Fischer and P. Bhattacharya, *J. Appl. Phys.* **96**, 4176 (2004).
62. "Nanoprobng of Semiconductor Heterointerfaces: Quantum Dots, Alloys, and Diffusion." R. S. Goldman, Invited Topical Review, *J. Phys. D.* **37**, R163 (2004).
63. "Formation and Blistering of GaAsN Nanostructure Layers." X. Weng, W. Ye, R. S. Goldman, and J. C. Mabon, *J. Vac. Sci. Technol.* **22**, 989 (2004).
64. "Monolithically integrated bacteriorhodopsin-GaAs/GaAlAs phototransceiver," J. Shin, P. Bhattacharya, J. Xu, et al., *Optics Lett.* **29**, 2264 (2004).
65. "Examination of an Unusual Grain Boundary in CaF<sub>2</sub>." M. E. Msall, W. Dietsche, R. Beane, R. Wichard, and J. Carpenter, *Phys. Stat. Solidi (c)* **1**, 2983 (2004).
66. "Ballistic Phonon-Drag Imaging in AlAs Quantum Wells." W. Dietsche, M. Msall, J.G.S. Lok, M. Lynass and M. Hauser, *Phys. Stat. Solidi (c)* **1**, 2947 (2004).
67. "Ultrafast Optical Generation of Coherent Phonons in CdTe<sub>1-x</sub>Se<sub>x</sub> Quantum Dots." A. V. Bragas, C. Aku-Leh, S. Costantino, A. Ingale, J. Zhao and R. Merlin, *Phys. Rev. B* **69**, 205306 (2004).
68. "Optical phonons in periodically inverted polar superlattice." J. Chen, J. B. Khurgin, *Phys. Rev. B* **70**, 085319 (2004).
69. "Picosecond Acoustic Phonon Pulse Propagation in Silicon," B. C. Daly, T. B. Norris, J. Chen and J. B. Khurgin, *Phys. Rev. B* **70**, 214307 (2004).
70. "Magnon Squeezing in an Antiferromagnet: Reducing the Spin Noise Below the Standard Quantum Limit." J. Zhao, A. V. Bragas, D. J. Lockwood and R. Merlin, *Phys. Rev. Lett.* **93**, 107203 (2004).
71. "Ultrafast Dynamic Control of Spin and Charge Density Oscillations in a GaAs Quantum Well." J. M. Bao, L. N. Pfeiffer, K. W. West and R. Merlin, *Phys. Rev. Lett.* **92**, 236601 (2004).
72. "Normal incidence intersubband photoresponse from phosphorus delta-doped Ge dots." S. Tong, H. J. Kim and K. L. Wang. *Appl. Phys. Lett.* **87**, 081104 (2005).
73. "Electrically injected spin-polarized vertical-cavity surface-emitting lasers," M. Holub, J. Shin, S. Chakrabarti, et al., *Appl. Phys. Lett.* **87**, 091108 (2005).
74. "Characteristics of a tunneling quantum-dot infrared photodetector operating at room temperature," P. Bhattacharya, X. H. Su, S. Chakrabarti, et al. *Appl. Phys. Lett.* **86**, 191106 (2005).
75. "Differential tunnel transparence of a rectangular heterostructural barrier for the terahertz frequency range." Z. Gribnikov and G. Haddad, *J. Appl. Phys.* **97**, 093705 (2005).
76. "Matrix Seeded Growth of Semiconductor Nanostructures using Ion Beams." X. Weng, W. Ye, S. Clarke, A. Daniel, V. Rotberg, R. Clarke, and R. S. Goldman, *J. Appl. Phys.* **97**, 064301 (2005).
77. "Differential tunnel transparency of a rectangular heterostructural barrier for the terahertz frequency range." Z. S. Gribnikov and G. I. Haddad, *J. Appl. Phys.* **97**, 093705 (2005).
78. "Stress Evolution in GaAsN Alloy Films." M. Reason, W. Ye, X. Weng, G. Obeidi, and R. S. Goldman, *J. Appl. Phys.* **97**, 103523 (2005).
79. "A comparative study of InAs quantum dot lasers with barriers of direct and indirect band gaps." G. Sun, R. A. Soref and J. B. Khurgin, *Microelectron. J.* **36**, 183 (2005)
80. "Laser in Physics: Squeezed Phonons in Solids." A. V. Bragas and R. Merlin, in *Encyclopedia of Modern Optics*, Vol. 4, ed. by B. Guenther, D. G. Steel and L. Bayvel (Academic Press, London, 2005), pp. 280-287.
81. "Ge dot mid-infrared photodetectors." S. Tong, J.Y. Lee, H. J. Kim, et al., *Optical Materials* **27**, 1097 (2005).
82. "Impulsive stimulated Raman scattering: Comparison between phase-sensitive and spectrally-filtered techniques." J. K. Wahlstrand, R. Merlin, X. Li, S. T. Cundiff and O. E. Martinez, *Optics Lett.* **30**, 926 (2005).
83. "Control of spin dynamics with laser pulses: Generation of entangled states of donor-bound electrons in a Cd<sub>1-x</sub>Mn<sub>x</sub>Te quantum well." J. M. Bao, A. V. Bragas, J. K. Furdyna and R. Merlin, *Phys. Rev. B* **71**, 045314 (2005).

84. "InP acoustic cavity phonon spectra probed by Raman scattering." M. F. Pascual Winter, A. Fainstein, M. Trigo, T. Eckhause, R. Merlin, A. Y. Cho and J. Chen, *Phys. Rev. B* **71**, 085305 (2005).
85. "Long-lived optical phonons in ZnO studied with impulsive stimulated Raman scattering." C. Aku-Leh, J. Zhao, R. Merlin, J. Menéndez and M. Cardona, *Phys. Rev. B* **71**, 205211 (2005). "Electron-phonon interaction via the Pekar mechanism in nanostructures." B. A. Glavin, V. A. Kochelap, T. L. Linnik, and K. W. Kim, *Phys. Rev B* **71**, 081305 (2005).
88. "Generation and propagation of a picosecond acoustic pulse at a buried interface: Time-resolved x-ray diffraction measurements." S. H. Lee, A. L. Cavalieri, D. M. Fritz, M. C. Swan, R. S. Hegde, M. Reason, R. S. Goldman and D. A. Reis, *Phys. Rev. Lett.* **95**, 246104 (2005).
89. "Impulsive Excitation of Cyclotron Oscillations in a Two-Dimensional Electron Gas." J. K. Wahlstrand, P. Jacobs, J. M. Bao, R. Merlin, K. W. West and L. N. Pfeiffer, *Solid State Commun.* **135**, 574-578 (2005); invited paper in a special issue on Fundamental Optical and Quantum Effects in Condensed Matter, ed. by E. Molinari, V. Pellegrini and A. Pinczuk.
90. "Simulations of the phonon Bragg switch in GaAs." J. M. H. Sheppard, P. Sondhaus, R. Merlin, P. Bucksbaum, R. W. Lee and J. S. Wark, *Solid State Commun.* **136**, 181-185 (2005).
91. "Active region design of a terahertz GaN/Al<sub>0.15</sub>Ga<sub>0.85</sub>N quantum cascade laser", G. Sun, R. A. Soref and J. B. Khurgin, *Superlattices & Microstructures* **37**, 107 (2005).
92. "Phonon Detection Using Quasi One-dimensional Quantum Wires," X. Bai, T. Eckhause, S. Chakrabarti, P. Bhattacharya, R. Merlin, and Ç. Kurdak, to be published in *Physica E* (2006).
93. "Optical Phonon Instability Induced by High-Speed Electron Transport in Nanoscale Semiconductor Structures," V. A. Kochelap, A. N. Klimov, and K. W. Kim, *Phys. Rev. B* **73**, 035301 (2006).
94. "Raman and ultrafast optical spectroscopy of acoustic phonons in CdTe<sub>0.68</sub>Se<sub>0.32</sub> quantum dots." A. V. Bragas, C. Aku-Leh and R. Merlin, *Phys. Rev. B* **73**, 125305 (2006).

## 6. PARTICIPATION/ PRESENTATIONS AT MEETINGS

1. "Amplification and generation of high-frequency coherent acoustic phonons under the drift of 2D-electrons." M. A. Stroschio, S. M. Komirenko, K. W. Kim, A. A. Demidenko, and V. A. Kochelap, in *Proceedings of the 25th Intl. Conf. on the Physics of Semiconductors*, edited by N. Miura and T. Ando (Springer, Berlin, 2001), Springer Proceedings in Physics Vol. **87**, pp. 873-874.
2. "Analysis of Electron Transport in a High Mobility Free-Standing GaN Substrate Grown by Hydride Vapor Phase Epitaxy." F. Yun, H. Morkoç, D. L. Rode, K. T. Tsen, L. Farina, Ç. Kurdak, S. S. Park, and K. Y. Lee, *Materials Research Society Proceedings* **680**, E 2.1 (2001).
3. "Coherent Phonon-Polaritons and Subluminal Cherenkov Radiation." J. K. Wahlstrand, T. E. Stevens, J. Kuhl and R. Merlin, to be published in *Physica B*; invited talk at the Tenth International Conference on Phonon Scattering in Condensed Matter, 2001, Hanover, NH.
4. "Coherent Intersubband Raman Beats in Modulation-Doped Quantum Wells." J. Bao, R. Merlin, K. W. West and L. N. Pfeiffer, at the March Meeting of the American Physical Society, 2001, Seattle, WA, *Bull. Amer. Phys. Soc.* **46**, 741 (2001).
5. "Electron Dispersion Relations with Negative Effective Mass in Quantum Wells Grown on the Cleaved Edge of a Superlattice." Z. S. Gribnikov, R. R. Bashirov, V. V. Mitin, H. Eisele and G. I. Haddad, presented at the 14th International Conference on the Electronic Properties of Two-Dimensional Systems, Prague, Czech Republic, 2001.
6. "In-plane thermal and electronic transport in quantum dot superlattices." A. Khitun, J. L. Liu, K. L. Wang and G. Chen, in *MRS proceedings* (2001).
7. "Ordinary and Extraordinary Refractive Indices of AlGaIn films in the Entire Composition Range." G. Webb-Wood, U. Ozgur, H. O. Everitt, F. Yun, T. King, and H. Morkoç, presented at the International Conference on Nitride Semiconductors, July 2001, Denver, CO.
8. "Quantum Well Based Phonon Detectors: Performance Analysis." X. Bai, Ç. Kurdak, S. Krishna and P. Bhattacharya, to be published in *Physica B*; presented at the Tenth International Conference on Phonon Scattering in Condensed Matter, 2001, Hanover, NH.

9. "Resonant excitation of coherent phonons in CdTe<sub>1-x</sub>Se<sub>x</sub> quantum dots." A. V. Bragas, S. Costantino, A. Ingale and R. Merlin, at the 2001 Quantum Electronics and Laser Science Conference, QELS'2001, OSA Technical Digest (Optical Society of America, Washington DC, 2001), p. 67.
10. "Study of Energy Relaxation in a GaN/AlGaN Heterostructure Using Thermal Noise Measurements." Ö. Süzer, T. Eckhause, A. Manasson, Ç. Kurdak, F. Yun, and H. Morkoç, presented at the 28<sup>th</sup> Annual Spring Symposium of the Michigan Chapter of the American Vacuum Society (2001).
11. "Study of Energy Relaxation and Heat Flow in GaN and GaN/AlGaN Heterostructure Using Thermal Noise Measurements." T. A. Eckhause, Ö. Süzer, A. Manasson, Ç. Kurdak, F. Yun and H. Morkoç, to be presented at the 2001 MRS Fall Meeting.
12. "Time-Resolved Anomalous Transmission of x-rays in Laser-heated Germanium." M. DeCamp, D. A. Reis, P. H. Bucksbaum, R. Clarke, E. Dufresne and R. Merlin, at the 2001 Quantum Electronics and Laser Science Conference, QELS'2001, OSA Technical Digest (Optical Society of America, Washington DC, 2001), p. 107.
13. "Coherent polaritons and Cerenkov radiation at subluminal speeds." T. E. Stevens, J. K. Wahlstrand, R. Merlin and J. Kuhl, at the 2001 Quantum Electronics and Laser Science Conference, QELS'2001, OSA Technical Digest (Optical Society of America, Washington DC, 2001), p. 152.
14. "Coherent intersubband oscillations in modulation-doped quantum wells." J. Bao, L. N. Pfeiffer, K. W. West and R. Merlin, at the 2001 Quantum Electronics and Laser Science Conference, QELS'2001, OSA Technical Digest (Optical Society of America, Washington DC, 2001), p. 248.
15. "Confinement and Amplification of Terahertz Acoustic Phonons in Cubic Heterostructures," S. M. Komirenko, K. W. Kim, V. A. Kochelap, and M. A. Stroschio, accepted for publication in the Proc. of the 10th Intl. Conf. on Phonon Scattering in Condensed Matter - Phonons 2001, Dartmouth, NH.
16. "Cherenkov generation of coherent LO phonons in quantum wells." S. M. Komirenko, K. W. Kim, V. A. Kochelap, I. Fedorov, and M. A. Stroschio, presented at the March Meeting of the American Physical Society (March, 2001, Seattle, Washington), Bull. Am. Phys. Soc. **46**, Z25.007 (2001).
17. "Quantum engineered electron dispersion relations in 2DEG on the cleaved edge of a superlattice." Z. S. Gribnikov, R. R. Bashirov, N. Z. Vagidov, V.V. Mitin, and G. I. Haddad, presented at. 2002 Intern. Conf. Phys. Semicond., Edinburg, UK (2002).
18. "Electric Field Induced Heating and Energy Relaxation in GaN." T. A. Eckhause, Ö. Süzer, Ç. Kurdak, F. Yun and H. Morkoç, Mat. Res. Soc. Proc. **693**, I11.25.1 (2002).
19. "Thermal Noise Measurements of Energy Relaxation and Heat Flow in n-type GaN." T. A. Eckhause, Ö. Süzer, Ç. Kurdak, F. Yun and H. Morkoç, presented at Seventh International Workshop on Wide-Bandgap III-Nitrides, Richmond, VA (2002).
20. "Quantum Well Based Phonon Detectors." X. Bai, Ç. Kurdak, S. Krishna, and P. Bhattacharya, Bull. Am. Phys. Soc. **47**, 770 (2002).
21. "Thermal Noise Measurements of Heating and Energy Relaxation in GaN." T. A. Eckhause, Ö. Süzer, Ç. Kurdak, F. Yun and H. Morkoç, Bull. Am. Phys. Soc. Bulletin **47**, 1073 (2002).
22. "Semiconductor quantum dot superlattice for coherent acoustic phonon emission." A. Khitun and K. L. Wang, Proc. 10th Int. Symp. Nanostructures: Physics and Technology (LOED), St. Petersburg, Russia (2002).
23. "Cherenkov Generation of Confined Acoustic and Optical Phonons in Quantum Wells." K. W. Kim, S. M. Komirenko, V. A. Kochelap, and M. A. Stroschio, Proc. SPIE **4643**, 77 (2002).
24. "Coherent LO phonon Generated by High-Velocity Electrons in Two-Dimensional Channels and Their Impact on Carrier Transport" S. M. Komirenko, K. W. Kim, V. A. Kochelap, and M. A. Stroschio, Proc. IEEE-NANO (2002).
25. "Dynamics of Spectral Hole Burning in Self-Organized Quantum Dot Amplifiers." T. B. Norris, invited talk presented at the OSA Topical Meeting on Nonlinear Optics, Hawaii (2002).
26. "Carrier Dynamics in In(Ga)As/Ga(Al)As Self-Organized Quantum Dots." P. Bhattacharya, T. Norris, and J. Singh, invited paper presented at Photonics West (2002).
27. "Evolution of Structure and Optical Properties of GaAsN Films Grown by Reactive Molecular Beam Epitaxy.", M. Reason, W. Ye, X. Weng, V. Rotberg, and R. S. Goldman, presented at Am. Vacuum Soc. Nat. Meeting (2002).
28. "Effects of Arsenic Flux on the Stress Evolution and Optical Properties of GaAsN Films Grown by Reactive Molecular Beam Epitaxy." M. Reason, W. Ye, X. Weng, and R. S. Goldman, presented at Electron. Mat. Conf. (2002).

29. "Ion-Cut-Synthesis of Narrow Gap Nitride Semiconductors." X. Weng, W. Ye, S. Clarke, A. Daniel, J. Holt, J. Sipowska, V. Rotberg, R. Clarke, A. Francis, and R. S. Goldman, presented at Electron. Mat. Conf. (2002).
30. "Ion-Cut-Synthesis of Narrow Gap Nitride Alloys." X. Weng, S. Clarke, W. Ye, A. Daniel, J. Holt, J. Sipowska, V. Rotberg, R. Clarke, A. Francis, and R. S. Goldman, presented at Mat. Res. Soc. Spring Meeting (2002).
31. "Synthesis, Microstructure, and Optical Properties of Narrow Gap Nitride Nanostructures." R. S. Goldman, presented at 7th Wide Bandgap III-Nitride Workshop (2002).
32. "Tunnel Injection Quantum Dot Lasers." S. Ghosh, P. Bhattacharya, J. Urayama, Z.-K. Wu, T. B. Norris, and K. Kamath." at CLEO, Long Beach, CA (2002).
33. "Gain Dynamics and Spectral Hole Burning in In(Ga)As Self-Organized Quantum Dots." K. Kim, J. Urayama, T.B. Norris, J. Singh, J. Phillips, and P. Bhattacharya, presented at QELS, Long Beach, CA (2002).
34. "Picosecond time-resolved x-ray diffraction probe of coherent lattice dynamics," D. A. Reis, M. F. DeCamp, P. H. Bucksbaum, R. Clarke, E. Dufresne and R. Merlin, at the Twelve National Synchrotron Radiation Instrumentation Conference, 2001, Madison, WI, Rev. Sci. Instrum. **73**,1361 (2002).
35. "Size-selective generation of coherent acoustic phonons in semiconductor nanocrystals." A. V. Bragas, C. Aku-Leh, J. Zhao and R. Merlin, Bull. Amer. Phys. Soc. **47**, 1267 (2002).
36. "Ultrafast Coherent Phonon Generation in Opaque Materials: Pump-Probe Asymmetry." J.-H. Choi, T. A. Eckhause, A. V. Bragas and R. Merlin, Bull. Amer. Phys. Soc., **47**, 994 (2002).
37. "Time-resolved Measurement of Temperature-Dependent Carrier Dynamics in Self-Organized InGaAs Quantum Dots." J. Urayama, T. B. Norris, H. Jiang, J. Singh, and P. Bhattacharya, presented at QELS, Long Beach, CA (2002).
38. "Gouy Phase Shift of Single-Cycle Picosecond Acoustic Pulses." N. C. R. Holme, M. T. Myaing, and T. B. Norris, presented at the Thirteenth International Conference on Ultrafast Phenomena, Vancouver, BC (2002).
39. "High-speed tunnel injection quantum dot lasers." S. Ghosh, Z-K. Wu, J. Singh, T. B. Norris, and P. Bhattacharya," presented at CLEO, Long Beach, CA (2002).
40. "Tunnel injection quantum dot lasers with large modulation bandwidth at room temperature." S. Ghosh, S. Pradhan, Z-K. Wu, J. Singh, T. B. Norris, and P. Bhattacharya, presented at the 60<sup>th</sup> Annual Device Research Conference, Santa Barbara, CA (2002).
41. "THz range unipolar ballistic tunnel-emission transit time oscillators." N. Z. Vagidov, J. East, V. V. Mitin and G. Haddad presented at the 14<sup>th</sup> International Symposium on Space Terahertz Technology, Tucson, AZ (2003).
42. "Development of Quantum Wire and Quantum Dot Tunable THz Phonon Detectors." X. Bai, K. M. Lewis, C. Kurdak, M. Msall, S. Krishna, and P. Bhattacharya, Bull. Am. Phys. Soc. **48**, 1000 (2003).
43. "Engineering nonradiative transition times in nitride QW's." J. B. Khurgin and G. Sun, Intersubband Transitions Conference, Evolene, Switzerland (2003).
44. "Semiconductor quantum dot superlattice for coherent acoustic phonon emission." Khitun A. and Wang K.L., Proceedings 10<sup>th</sup> Int. Symp. Nanostructures: Physics and Technology, LOED, St. Petersburg, Russia (2002); SPIE-Int. Soc. Opt. Eng. Proceedings of Spie - the International Society for Optical Engineering **5023**, 368-71 (2003).
45. "Stress Evolution and Nitrogen Incorporation in GaAsN Films." M. Reason, W. Ye, X. Weng, G. Obeidi, R.S. Goldman, and V. Rotberg, Oral Presentation at the International Conference on Compound Semiconductors, August 2003.
46. "Controlled Fabrication of Electrodes with a few Nanometer Spacing for the Study of Electrical Transport through Thiol-Coated Au Nanoparticles." J. Kim, L.A. Farina, K.M. Lewis, X. Bai, C. Kurdak, M.P. Rowe, A.J. Matzger, M. Reason, and R.S. Goldman, presentation at IEEE-Nano (2003).
47. "Generation and Propagation of Coherent THz Folded Acoustic Phonons." T. A. Eckhause, J. K. Wahlstrand, R. Merlin, M. Reason, and R.S. Goldman, oral presentation at CLEO/QUELS 2003.
48. "Phonon Lasers." J. B. Khurgin and J. Chen, at QUELS-2003, Baltimore (2003).
49. "Stress Evolution in GaAsN Films Grown by Reactive Molecular Beam Epitaxy." M. Reason, W. Ye, X. Weng, G. Obeidi, R.S. Goldman, V. Rotberg, oral presentation at the International Conference on the Formation of Semiconductor Interfaces, Madrid, Spain, September 2003.
50. "Phonon Lasers." J. B. Khurgin and J. Chen, at QUELS-2003, Baltimore (2003).

51. "Engineering nonradiative transition times in nitride QW's." J. B. Khurgin and G. Sun, Intersubband Transitions Conference, Evolene, Switzerland (2003).
52. "Anisotropic Stress Relaxation and Ordering of InAs/GaAs Quantum Dot Superlattices." W. Ye, S. Hanson, M. Reason, X. Weng, and R.S. Goldman, Oral Presentation at the 2003 International Symposium of the AVS Science and Technology Society, November 2003.
53. "Stress Evolution and Nitrogen Incorporation in GaAsN Films Grown by Reactive Molecular Beam Epitaxy." M. Reason, W. Ye, X. Weng, G. Obeidi, V. Rotberg, and R. S. Goldman, Oral Presentation at the 2003 International Symposium of the AVS Science and Technology Society, November 2003.
54. "Effects of InAlSb Buffer Layers on the Structural and Electronic Properties of InSb Films." X. Weng, N.G. Rudawski, R. S. Goldman, D.L. Partin, and J. Heremans, Oral Presentation at the 2003 International Symposium of the AVS Science and Technology Society, November 2003.
55. "Stress Relaxation and Ordering of InAs/GaAs Quantum Dot Superlattices." W. Ye, S. Hanson, M. Reason, X. Weng, and R. S. Goldman, Oral Presentation at the Fall 2003 Meeting of the Materials Research Society, December 2003.
56. "THz range unipolar ballistic tunnel-emission transit time oscillators." N. Z. Vagidov, J. East, V. V. Mitin and G. Haddad presented at the 14<sup>th</sup> International Symposium on Space Terahertz Technology, Tucson, AZ (2003).
57. "Controlled Fabrication of Electrodes with a Few Nanometer Spacing by Selective Etching of GaAs/AlGaAs Heterostructure." J. Kim, L. A. Farina, K. M. Lewis, X. Bai, Ç. Kurdak, M. Reason, and R. S. Goldman Proceedings of 2003 Third IEEE Conference on Nanotechnology 2, 599 (2003).
58. "Development of Quantum Wire and Quantum Dot Tunable THz Phonon Detectors." X. Bai, K. M. Lewis, Ç. Kurdak, M. Msall, S. Krishna, and P. Bhattacharya, Bull. Am. Phys. Soc. 48, 1000 (2003).
59. "Stress Evolution in GaAsN Films Grown by Reactive Molecular Beam Epitaxy." M. Reason, W. Ye, X. Weng, G. Obeidi, V. Rotberg, and R.S. Goldman, Proceedings of the National Center for Photovoltaics and Solar Program Review Meeting (2003).
60. "Stress Evolution in GaAsN Films Grown by Reactive Molecular Beam Epitaxy." M. Reason, W. Ye, X. Weng, G. Obeidi, R.S. Goldman, V. Rotberg, oral presentation at the International Conference on the Formation of Semiconductor Interfaces, Madrid, Spain (2003).
61. "Semiconductor quantum dot superlattice for coherent acoustic phonon emission." Khitun A. and Wang K.L., Proceedings 10<sup>th</sup> Int. Symp. Nanostructures: Physics and Technology, LOED, St. Petersburg, Russia (2002); SPIE-Int. Soc. Opt. Eng. Proceedings of Spie - the International Society for Optical Engineering 5023, 368-71 (2003).
62. "Controlled Fabrication of Electrodes with a few Nanometer Spacing for the Study of Electrical Transport through Thiol-Coated Au Nanoparticles." J. Kim, L.A. Farina, K.M. Lewis, X. Bai, C. Kurdak, M.P. Rowe, A.J. Matzger, M. Reason, and R.S. Goldman, presentation at IEEE-Nano (2003).
63. "Generation and Propagation of Coherent THz Folded Acoustic Phonons." T. A. Eckhause, J. K. Wahlstrand, R. Merlin, M. Reason, and R.S. Goldman, oral presentation at CLEO/QUELS 2003.
64. "Lateral and Height Distributions of Self-Assembled InGaAs Quantum Dots on GaAs Substrates." Roshko, S.Y. Lehman, R.P. Mirin, K.D. Cobry, W. Ye, M. Reason, X. Weng, and R. S. Goldman, Oral Presentation at the Fall 2003 Meeting of the Materials Research Society, December 2003.
65. "Controlled Fabrication of Electrodes with a Few Nanometer Spacing by Selective Etching of GaAs/AlGaAs Heterostructure." J. Kim, L. A. Farina, K. M. Lewis, X. Bai, Ç. Kurdak, M. Reason, and R. S. Goldman, Proceedings of 2003 Third IEEE Conference on Nanotechnology, Vol. 2, 599 (2003).
66. "Theory of heterostructural tunnel emitters for ballistic transit-time terahertz-range oscillators." Z. Gribnikov and G. Haddad, Proceedings of 27<sup>th</sup> Int. Conf. Phys. Semicond (ICPS-27), July 26-30, 2004, Flagstaff, Arizona, USA..
67. "Pekar mechanism of electron-phonon interaction in nanostructures." B. A. Glavin, V. A. Kochelap, T. L. Linnik, and K. W. Kim, Intl. Conf. on Phonon Scattering in Condensed Matter, St.-Petersburg, 2004; Book of Abstracts, p. 104.
68. "Ultrafast Strain Propagation in Epitaxial Thin Films." D. Fritz, S.-H. Lee, A. Cavalierie, D. Reis, R. Hegde, and R. S. Goldman, oral presentation at the American Physical Society Meeting, March 2004.
69. "High Frequency (THz) Sound Propagation in Semiconductor Structures." M. Trigo, T.A. Eckhause, J.K. Wahlstrand, R. Merlin, M. Reason, and R.S. Goldman, oral presentation at the American Physical Society Meeting, March 2004.

70. "Picosecond x-ray Diffraction Study of Strain Propagation in Epitaxial Thin Films." S.-H. Lee, A. Cavaliere, D.M. Fritz, R. Hegde, R.S. Goldman, and D.A. Reis, presentation at the Workshop on Ultrafast x-ray Science, April 2004
71. "Stress Evolution in Dilute GaAsN Alloys Films." M. Reason, W. Ye, X. Weng, D. Dettling, S. Hanson, G. Obeidi, and R.S. Goldman, Poster Presentation at AVS-MI Spring Symposium, May 2004.
72. "Effects of Buffer Layer Patterning on Lateral Ordering of InAs/GaAs Quantum Dot Superlattices." W. Ye, M. Reason, X. Weng, and R.S. Goldman, Poster Presentation at AVS-MI Spring Symposium, May 2004.
73. "{113} Defect-Engineered Silicon Light-Emitted Diodes." G. Z. Pan, R. P. Ostroumov, Y. Lian, K. N. Tu and K. L. Wang, to appear in IEDM 2004 Proceedings
74. "Thermal conductivity of Si/Ge quantum dot superlattices." A. Khitun and K. L. Wang, *Proc. IEEE NANO 2004*, Munich, August 2004.
75. "Scanning Tunneling Microscopy Studies of GaAsN Film Growth." N.G. Rudawski, X. Weng, H.A. McKay, and R.S. Goldman, Poster Presentation at AVS-MI Spring Symposium, May 2004.
76. "Nitrogen Incorporation in GaAsN Films and GaAsN/GaAs Superlattices." H. McKay, M. Reason, X. Weng, N. Rudawski, W. Ye, R. S. Goldman, and V. Rotberg, Poster Presentation at the AVS-MI Spring Symposium, May 2004.
77. "Nitrogen Incorporation in Dilute GaAsN Alloy Films." M. Reason, H. McKay, X. Weng, N. Rudawski, R.S. Goldman, and V. Rotberg, Oral Presentation at Symposium M of the European MRS (E-MRS), May 2004.
78. "Effect of Arsenic Species and Si-doping on N Incorporation in GaAsN Films." M. Reason, H. McKay, X. Weng, N. Rudawski, W. Ye and R.S. Goldman, oral presentation at the Electronic Materials Conference, June 2004.
79. "Nitrogen Incorporation in GaAsN Films and GaAsN/GaAs Superlattices." H. McKay, M. Reason, X. Weng, N. Rudawski, W. Ye, R.S. Goldman, and V. Rotberg, Oral Presentation at the AVS National Symposium, November 2004.
80. "Buffer Layer Patterning of InAs/GaAs Quantum Dot Superlattices." W. Ye, S. Hanson, X. Weng, and R.S. Goldman, oral presentation at the MRS Fall Meeting, December 2004.
81. "Scanning Tunneling Microscopy Studies of GaAsN Film Growth." N.G. Rudawski, X. Weng, H.A. McKay, and R.S. Goldman, Poster Presentation at the MRS Fall Meeting, December 2004.
82. "Theory of heterostructural tunnel emitters for ballistic transit-time terahertz-range oscillators." Z. S. Gribnikov and G. I. Haddad, *Proceedings of the 27<sup>th</sup> Int. Conf. on the Phys. Semicond. (ICPS-27, 2004)*, [AIP Conference Proceedings v.772, pp. 1200 -1200, Melville, NY, 2005].
83. "Generation and Remote Detection of Coherent Folded Acoustic Phonons." M. Trigo, T. A. Eckhause, J. K. Wahlstrand, R. Merlin, M. Reason and R. S. Goldman, in *Proceedings of the 27th International Conference on the Physics of Semiconductors*, Vol. , ed. by J. Menéndez and C. G. Van de Walle (AIP Conference Proceedings, 2005), pp. ; presented at the 27th International Conference on the Physics of Semiconductors, 2004, Flagstaff, AZ, USA.
84. "Optical generation of many-spin entangled states in a quantum well." R. Merlin, J. M. Bao, A. V. Bragas and J. K. Furdyna, in *Noise and Information in Nanoelectronics, Sensors and Standards II*, ed. by J. M. Smulko, Y. Blanter, M. I. Dykman and L. B. Kish, SPIE Proceedings 5472, pp. 200-213; keynote talk at the SPIE (The International Society for Optical Engineering) 2004 Second International Symposium on Fluctuations and Noise, 2004, Gran Canaria, Spain.
85. "Analysis and design of terahertz transit-time diodes." X. Bi, J. R. East, U. Ravaioli and G. Haddad, presented at 16<sup>th</sup> International Conference on Space Terahertz Technology, Chalmers University of Technology, Goteburg, Sweden, May, 2005
86. "Anharmonic Interactions in ZnO Probed with Impulsive-Stimulated Raman Scattering." C. Aku-Leh, J. Zhao, R. Merlin, J. Menéndez and M. Cardona, in *Physics of Semiconductors*, ed. by J. Menéndez and C. G. Van de Walle, AIP Conference Proceedings 772 (2005), pp. 1128-1129; presented at the 27th International Conference on the Physics of Semiconductors, 2004, Flagstaff, AZ, USA.
87. "Generation and Remote Detection of Coherent Folded Acoustic Phonons." M. Trigo, T. A. Eckhause, J. K. Wahlstrand, R. Merlin, M. Reason and R. S. Goldman, in *Physics of Semiconductors*, ed. by J. Menéndez and C. G. Van de Walle, AIP Conference Proceedings 772 (2005), pp. 1190-1191; presented at the 27th International Conference on the Physics of Semiconductors, 2004, Flagstaff, AZ, USA.

88. "Observation of Coherent Hybrid Intersubband-Cyclotron Modes in a Quantum Well." J. K. Wahlstrand, D. M. Wang, P. Jacobs, J. M. Bao, R. Merlin, K. W. West and L. N. Pfeiffer, in *Physics of Semiconductors*, ed. by J. Menéndez and C. G. Van de Walle, AIP Conference Proceedings 772 (2005), pp. 1313-1314; presented at the 27th International Conference on the Physics of Semiconductors, 2004, Flagstaff, AZ, USA.
89. "Optically-Generated Many Spin Entanglement in a Quantum Well." J. Bao, A. V. Bragas, J. K. Furdyna and R. Merlin, in *Physics of Semiconductors*, ed. by J. Menéndez and C. G. Van de Walle, AIP Conference Proceedings 772 (2005), pp. 1429-1430; presented at the 27th International Conference on the Physics of Semiconductors, 2004, Flagstaff, AZ, USA.
90. "Ultrafast generation of optical and acoustic phonons in nanocrystallites." A. V. Bragas, C. Aku-Leh and R. Merlin, in *Ultrafast Phenomena in Semiconductors and Nanostructure Materials IX*, ed. by K. -T. Tsen, J. -J. Song and H. Jiang, SPIE Proceedings 5725, pp. 126-135; invited talk at Photonics West 2005, Symposium on Optoelectronic Materials and Devices.
91. "Influence of Nitrogen Incorporation Mechanisms on Electrical Properties of GaAsN Alloys," H. A. McKay, M. Reason, D. Mao, X. Bai, Ç. Kurdak, V. Rotberg, and R. S. Goldman, *Bull. Am. Phys. Soc.* 50, 392 (2005).
92. "Two-Dimensional Electron Transport in Selectively Doped GaAsN/AlGaAs Heterostructures," X. Bai, H. A. McKay, R. S. Goldman, and Ç. Kurdak, *Bull. Am. Phys. Soc.* 50, 392 (2005).

## 7. PATENT DISCLOSURES

X. Weng and R. S. Goldman, "Narrow Energy Band Gap GaAsN Semiconductors and an Ion-Cut-Synthesis Method for Producing the Same." United States Patent 7,056,815.

## 8. HONORS AND AWARDS

Pallab K. Bhattacharya is a Fellow of IEEE. He received the Certificate of Recognition for Technical Innovation, NASA, 1993, the John Simon Guggenheim Award, 1998, the IEEE (LEOS) Distinguished Lecturer Award, 1998, and the S. S. Attwood Award, University of Michigan, 1999. In 2002, he was the recipient of the OSA Nick Holonyak, Jr. Award.

Cagliyan Kurdak was the recipient of the Alfred P. Sloan Fellowship in 2000 and the Harold C. Early Award in 2003.

George I. Haddad received the 1970 Curtis W. McGraw Research Award of the American Society for Engineering Education for outstanding achievements by an engineering teacher, the College of Engineering Excellence in Research Award (1985), the Distinguished Faculty Achievement Award (1986) of The University of Michigan, and the S. S. Attwood Award of the College of Engineering for outstanding contributions to Engineering education, research and administration. He is also the recipient of the 1996 IEEE-MTT Distinguished Educator Award. He is a Fellow of the IEEE and a member of the National Academy of Engineering.

Roberto Merlin is a Fellow of the American Physical Society, the Optical Society of America and the von Humboldt Foundation (Germany). In 1997, he received the Dean's Faculty Award of the College of Literature, Science and the Arts, University of Michigan. He is also the recipient of the 2006 Frank Isakson Prize of the American Physical Society for Optical Effects in Solids.

Hadis Morkoç is a Fellow of the IEEE, the American Association for the Advancement of Science, and the American Physical Society.

Kang L. Wang is a Fellow of the IEEE. He has received several awards including the Semiconductor Research Corporation Inventor Award (consecutively from 1989 through 1994, and again from 1996 through 1998). In 1995 he was also honored with the Semiconductor Research Corporations Technical Excellence Award. Other honors include the J.H. Ahlers Achievement Award and the John Simon Guggenheim Fellow Award.

Rachel Goldman was the recipient of the 2002 Peter Mark Memorial Award, presented by the American Vacuum Society to a young scientist or engineer for outstanding theoretical or experimental work.

Three of our co-PIs, R.S. Goldman, P.K. Bhattacharya, and T. Norris, with J. Singh won the Ted Kennedy Family Team Excellence Award, UM College of Engineering in 2004.

**Awards to students associated with the project:**

Scott Hanson (undergraduate student), Award Winner, 2004 Undergraduate Student Research Award, the AVS Science and Technology Society; 2004 Henry Ford II Prize, UM

Nick Rudawski (undergraduate student) 2004 Andrew A. Kucher Award, presented to a graduating senior who has made outstanding contributions to engineering research at the University of Michigan